Properties of High-Energy Solar Particle Events Associated with Solar Radio Emissions

Dheyaa Ameri[1,2] [ID] · **Eino Valtonen**[1] [ID] ·
Silja Pohjolainen[1]

Abstract We have analysed 58 high-energy proton events and 36 temporally related near-relativistic electron events from the years 1997–2015 for which the velocity dispersion analysis of the first-arriving particles gave the apparent path lengths between 1 and 3 AU. We investigated the dependence of the characteristics of the proton events on the associations of type II, III, and IV radio bursts. We also examined the properties of the soft X-ray flares and coronal mass ejections associated with these events. All proton events were associated with decametric type III radio bursts, while type IV emission was observed only in the meter wavelengths in some of the events (32/58). Almost all proton events (56/58) were associated with radio type II bursts: 11 with metric (m) type II only, 11 with decametric–hectometric (DH) only, and 34 with type II radio bursts at both wavelength ranges. By examining several characteristics of the proton events, we discovered that the proton events can be divided into two categories. The characteristics of events belonging to the same category were similar, while they significantly differed between events in different categories. The distinctive factors between the categories were the wavelength range of the associated type II radio emission and the temporal relation of the proton release with respect to the type II onset. In Category 1 are the events which were associated with only metric type II emission or both m and DH type II and the release time of protons was before the DH type II onset (18/56 events). Category 2 consists of the events which were associated with only DH type II emission or both m and DH type II and the protons were released at or after the DH type II onset (31/56 events). For seven of the 56 events we were not able to determine a definite category due to timing uncertainties. The events in Category 1 had significantly higher intensity rise rates, shorter rise times, lower release heights, and harder energy spectra than

✉ D. Ameri
  dahame@utu.fi

  E. Valtonen
  eino.valtonen@utu.fi

  S. Pohjolainen
  silpoh@utu.fi

[1] Department of Physics and Astronomy, University of Turku, 20014 Turku, Finland

[2] Department of Ecology, University of Basra, Karmat Ali B.P49, Basra, Iraq

 Springer

Category 2 events. Category 1 events also originated from magnetically well-connected regions and had only small time differences between the proton release times and the type III onsets. The soft X-ray flares for these events had significantly shorter rise times and durations than for Category 2 events. We found 36 electron events temporally related to the proton events, which fulfilled the same path length criterion as the proton events. We compared the release times of protons and electrons at the Sun, and discovered that in 19 of the 36 events protons were released almost simultaneously (within ± 7 minutes) with the electrons, in 16 events protons were released later than the electrons, and in one event electrons were released after the protons. The simultaneous proton and electron events and the delayed proton events did not unambiguously fall in the two categories of proton events, although most of the events in which the protons were released after the electrons belonged to Category 2. We conclude that acceleration of protons in Category 1 events occurred low in the corona, either by CME-driven shocks or below the CMEs in solar flares or in CME initiation related processes. It seems plausible that protons in Category 2 events were accelerated by CME-driven shocks high in the solar corona. Large delays of protons with respect to type III onsets in the events where protons were released after the electrons suggest late acceleration or release of protons close to the Sun, but the exact mechanism causing the delay remained unclear.

Keywords Energetic particles, protons, electrons · Radio emissions · Coronal mass ejections · Flares

1. Introduction

Solar energetic particles (SEPs) are accelerated at the Sun or in the interplanetary medium during solar flares and coronal mass ejections, and propagate along interplanetary magnetic field lines from the Sun to the Earth. SEPs can reach energies of several GeV nucleon^{-1} and occur in events that last from some hours to a few days with intensity enhancements above the quiet-time background by many orders of magnitude. Based on the signatures in soft X-rays, SEP events are often divided into two classes (Cane, McGuire, and von Rosenvinge, 1986): impulsive events, which have high electron-to-proton ratios, are related to solar flares, and occur low in the corona, and gradual events, in which particles can be accelerated up to much higher energies in coronal mass ejection (CME)-driven shocks, and occur high in the corona (Reames, 1999).

Radio emission can be used as a probe to trace particle acceleration in the solar corona and interplanetary space. Electrons accelerated in solar flares and propagating along open magnetic field lines outward from the Sun are the source of type III solar radio bursts (Lin, 1985). Type II radio bursts are produced by electrons accelerated in magnetohydrodynamic shocks propagating from low corona into interplanetary space with the emission frequency slowly drifting from high to lower frequencies due to decreasing electron density encountered by the shock in the corona (Cairns *et al.*, 2003). The starting frequencies of metric type II bursts are typically ~ 100 MHz corresponding to the height of ~ 1.5 R$_\odot$ from the Sun center. Type II emission in the decametric–hectometric wavelength domain is typically observed at frequencies below ~ 10 MHz originating from heights above ~ 3 R$_\odot$. Since electrons are accelerated in shocks driven by coronal mass ejections, it is believed that protons as well can be accelerated. Type IV bursts are quasi-continuum radio emissions caused by energetic electrons trapped within magnetic structures and plasma (Benz, 1980). Metric type IV bursts can be classified into two categories, stationary and moving. The former show no systematic movement and their sources may be energetic particles trapped in post-

flare loops and arcades. The latter show frequency drifts toward the lower frequencies, and their sources are mostly energetic particles trapped in rising CME structures (see Nindos *et al.*, 2008). Rarely the moving type IV bursts extend in dynamic spectra to the hectometric wavelengths, and their characteristics were recently studied by Hillaris, Bouratzis, and Nindos (2016).

It has been established that the occurrence of high-energy (> 20 MeV) solar proton events is well correlated with type II radio emission. Cliver, Kahler, and Reames (2004) investigated metric type II bursts with western-hemisphere sources and discovered that 25% of the bursts observed only at metric wavelengths were associated with solar energetic particle events at Earth, but the association increased to $\sim 90\%$, when the metric type II bursts were accompanied by decametric–hectometric type II emission. Also Gopalswamy (2003) and Gopalswamy *et al.* (2005) have shown that a vast majority of solar particle events is associated with type II bursts at decametric–hectometric and longer wavelengths. Cliver, Kahler, and Reames (2004) concluded that shock acceleration in the solar atmosphere is strongest at heights above ~ 3 R$_\odot$. In a study of release times of energetic particles in ground level enhancement events, Reames (2009) found that the release of particles in all events occurred after the onset of the metric type II radio emission and the release in well-connected events began at the height of $2 – 4$ R$_\odot$ over a longitude span of $\sim 100°$ and moved to greater heights at longitudes more distant from the source. For 44 high-energy proton events associated with type II bursts, Kouloumvakos *et al.* (2015) reported relatively broad distribution of release heights extending up to 8 R$_\odot$ with a maximum between $3 – 4$ R$_\odot$.

There are indications that protons and electrons may not be accelerated by the same mechanisms and released simultaneously, but that the acceleration or release of one or the other species may be delayed by some mechanism. Krucker and Lin (2000) showed that low-energy proton events appeared in two classes. Protons in the first class had path lengths in the range $1.1 – 1.3$ AU, the same as the electrons in the temporally related events, while protons in the second class had apparent path lengths around 2 AU. The protons in the first class were released $\sim 0.5 – 2$ hours after the electrons, and assuming proton acceleration in CME-driven shocks Krucker and Lin (2000) concluded that the protons at all energies were accelerated simultaneously high in the corona, roughly $\sim 1 – 10$ R$_\odot$ above the electrons. The apparently longer path lengths of protons of the second class were interpreted to be a consequence of a successively later release of protons at successively lower energies, thus leading to later onset times at 1 AU. In a study of 34 high-energy proton events accompanied by type II, III, or IV (continuum) radio emission and electron events, Kouloumvakos *et al.* (2015) found that in roughly half of the events protons and electrons were released simultaneously, but in the other half electron release was delayed compared to proton release on average by ~ 7 minutes. They also found that the electron release occurred on the average ~ 12.3 minutes after the start of type III burst, but pointed out that the type III onset and release times of high-energy protons and electrons did not show a dominant sequence. In a recent study of 23 large SEP events, Xie *et al.* (2016) found that in most cases near-relativistic electrons and high-energy protons were released at the same time within 8 minutes. In some events, however, large delays occurred for both relativistic electrons and protons relative to lower-energy (0.5 MeV) electrons. Xie *et al.* (2016) suggested that either the time needed for the shock to reach sufficient strength for efficient acceleration or particle transport effects caused the observed delays.

In this article we analyze 58 proton events and 36 temporally related electron events. We compare the release times of protons and electrons and investigate the characteristics of the proton events and their associations with type II, III, and IV radio emissions. Section 2 defines the data sources and describes the analysis methods. Section 3 presents the results of velocity dispersion analysis (VDA) of $13 – 80$ MeV protons and $20 – 646$ keV electrons with

their relative release times and path lengths. In Section 4 we discuss the associations and relative timing of type II, III, and IV radio bursts with the particle events. We define two categories of proton events and discuss the temporally related electron events. The properties of the proton events in the two categories are presented in Section 5. The results are summarized in Section 6 and discussed in Section 7. Conclusions in Section 8 complete the article.

2. Data Sources and Analysis Methods

The catalog of Paassilta *et al.* (2017) was used to select the proton events for this study. The catalog consists of proton events observed by the *Energetic and Relativistic Nuclei and Electron* experiment (ERNE) (Torsti *et al.*, 1995) on board the *Solar and Heliospheric Observatory* (SOHO) spacecraft at energies $55 – 80$ MeV during the years $1996 – 2016$. From this catalog we selected for analysis those events for which the velocity dispersion analysis gave apparent path lengths between $1 – 3$ AU. For VDA we used 1-minute averages in eight energy channels of ERNE[1] extending from 13.8 MeV up to 80.3 MeV. These channels were selected because they have the highest counting statistics and usually are least affected by the pre-event backgrounds, thus allowing reliable determination of the onset times. For electrons we used the omnidirectional electron data[2] from the *3-D Plasma and Energetic Particle Investigation* (3DP) (Lin *et al.*, 1995) spectroscopic survey telescopes on board the *Wind* spacecraft. The electron energies covered the range $60 – 646$ keV in seven energy channels with 12-second time resolution.

Wind/Plasma and Radio Waves (WAVES) (Bougeret *et al.*, 1995) data[3] were searched for decametric type III radio bursts associated with the selected proton events. For associating type II radio bursts with the events we used the lists compiled by the *Wind* and STEREO data center[4] for decametric–hectometric (DH) type II, and *Solar Geophysical Data* (SGD)[5] for metric (m) type II bursts. The most recent dates, with no listed m type II bursts available from the catalogs, were checked from the radio dynamic spectra provided by the *Radio Solar Telescope Network* (RSTN), *Hiraiso Radio Spectrograph* (HiRAS), *Green Bank Solar Radio Burst Spectrometer* (GBSRBS), *Bruny Island Radio Spectrometer* (BIRS), and *Nancay Decameter Array* (NDA). We used radio dynamic spectra and spectral listings from different ground-based stations to find m type IV bursts associated with our events, and the DH type IV catalog of Hillaris, Bouratzis, and Nindos (2016) and *Wind*/WAVES spectral data for more recent events to find DH type IV bursts. The data for solar soft X-ray flares were obtained from the *Geostationary Operational Environmental Satellites* (GOES).[6] The CME catalog[7] of the *Large Angle and Spectrometric Coronagraph* (LASCO) (Brueckner *et al.*, 1995) on board SOHO was used to find the characteristics of the CMEs associated with the proton events.

We used the Poisson-CUSUM method (Huttunen-Heikinmaa, Valtonen, and Laitinen, 2005) to determine the onset times of the first-arriving protons and electrons observed by SOHO/ERNE and *Wind*/3DP, respectively. The cumulative control scheme used in Poisson-

---

[1] https://srl.utu.fi/erne_data/.

[2] https://wind.nasa.gov/data_sources.php.

[3] http://cdaw.gsfc.nasa.gov/images/wind/waves/.

[4] https://solar-radio.gsfc.nasa.gov/wind/data_products.html.

[5] https://www.ngdc.noaa.gov/stp/solar/solar-features.html.

[6] https://hesperia.gsfc.nasa.gov/goes/goes_event_listings/.

[7] https://cdaw.gsfc.nasa.gov/CME_list/index.html.

CUSUM cumulates the difference between the observed counting rate at a selected energy and a reference value. When this cumulation equals or exceeds a decision interval value, an out-of-control signal is generated. The reference value is calculated by using a 60-minute moving average of the background counting rate. To avoid false alarms but still retain the sensitivity, we require that after the first five consecutive out-of-control signals, the signal is also generated for at least 22 of the next 25 observations. The time of the first out-of-control signal is then taken as the onset time of the event at the inspected energy. For more details of the method, see Huttunen-Heikinmaa, Valtonen, and Laitinen (2005).

Velocity dispersion analysis gives an estimate of the solar release time of the particles at the acceleration site close to the Sun. VDA relies on the assumptions that particles at all energies are simultaneously released from the same acceleration site in the solar corona, and that the propagation of the first-arriving particles along the interplanetary magnetic field lines connecting the observer near 1 AU to the acceleration site is scatter-free. Thus, the higher energy particles are expected to arrive earlier than the lower-energy particles, and there is a linear relationship between the observed onset times of an event at different energies and the corresponding reciprocal speeds of the particles. The velocity dispersion equation can be written as

$$t_{\text{onset}}(E) = t_{\circ} + 8.33(\text{min/AU})s\beta^{-1}(E), \tag{1}$$

where $t_{\text{onset}}(E)$ is the onset time at proton kinetic energy E, $t_{\circ}$ is the release time at the Sun, s is the apparent path length (AU) traveled by the particle, and $\beta^{-1} = c/v(E)$ is the reciprocal speed of the particle. The slope of a linear fit of Equation 1 gives the apparent path length traveled by the particle, and the interception of the fit line with the ordinate axis gives the release time of the particle at the acceleration site close to the Sun. We estimated the statistical uncertainties of the onset times by using a similar method as Kouloumvakos *et al.* (2015). For each energy used in the VDA, we randomly sampled with replacement the pre-event background. We did this 1000 times and for each iteration we used the Poisson-CUSUM method to determine the onset time. As the final onset time we used the average of the 1000 iterations and three standard deviations of the distribution as the uncertainty. For proton onset times the uncertainties were typically of the order of 10 minutes and for electrons a few minutes. The uncertainties used for the reciprocal speeds of the particles corresponded to the widths of the respective energy channels.

The Williamson–York method (Williamson, 1968; York *et al.*, 2004) was used for the linear fit of the onset times *vs.* reciprocal speeds by using a spreadsheet provided by Cantrell (2008). This method is a bivariate weighted fit allowing statistical uncertainties in both variables. The results were further verified by using the MPFITEXY routine (Williams, Bureau, and Cappellari, 2010) implemented in IDL, which depends on the MPFIT package (Markwardt, 2009). Both fitting methods produced release times and path lengths of particles with only insignificant differences (< 2 minutes and < 0.05 AU absolute average deviations for protons and < 1 minute and < 0.06 AU for electrons). In all analyses presented below, we use the standard deviations of the linear fit parameters as the uncertainties of the estimated release times and path lengths.

3. Velocity Dispersion Analysis

3.1. High-Energy Proton Events

We performed velocity dispersion analysis for all the 175 high-energy proton events in the catalog of Paassilta *et al.* (2017) using the eight most reliable energy channels of ERNE

in the range 13.8 – 80.3 MeV. Several studies (*e.g.* Lintunen and Vainio, 2004; Kahler and Ragot, 2006; Vainio *et al.*, 2013; Kouloumvakos *et al.*, 2015; Xie *et al.*, 2016) have concluded that when using VDA to derive the release times of particles, the results are most trustworthy for events for which VDA yields apparent path lengths typically in the range ≈ 1 – 3 AU. However, interplanetary scattering, if present, can still deteriorate the accuracy of the results (Sáiz *et al.*, 2005; Laitinen *et al.*, 2015). We selected for analysis the proton events for which VDA gave apparent path lengths in the range 1 – 3 AU to achieve as good reliability as possible. This criterion excluded many events from the catalog of Paassilta *et al.* (2017). In some cases, data gaps prevented VDA altogether or there were intensity fluctuations at the time of the onset leading to clearly unphysical apparent path lengths. Also, in many events either due to the background from previous events or due to very slowly rising intensities, the Poisson-CUSUM method failed to yield definite onset times. For 70 proton events we found an apparent path length in the range 1 – 3 AU. During twelve of these events SOHO was at the 180° roll attitude, meaning that instead of looking at the direction of the nominal Parker spiral field line ERNE was looking at 45° to the east from the Sun–Earth line. Under these circumstances ERNE might not have seen the first-arriving particles leading to unknown uncertainties in the derived release times and apparent path lengths. Therefore, we excluded these events from the analysis and were left with 58 proton events. The apparent path lengths and release times (8.33 min added) with error estimates are given in Table 2 in the Appendix for these events together with the onset times of the associated solar radio emissions, soft X-ray flare onset times, locations, and connection angles (see Section 5.1), and times of first observations of CMEs. The X-ray flare classes and CME speeds and widths are not listed in Table 2, but the sources of these parameters used in the analyses were those referenced above.

With the above selection criterion of the events, the average apparent path length of protons and its standard error (standard deviation of the mean) in the 58 high-energy events were found to be (1.50 ± 0.05) AU. The path length distribution had a prominent maximum in the range 1.3 – 1.4 AU with the tail extending to 2.5 AU.

The time–intensity profiles of two proton events together with the VDA results are shown in Figure 1. The proton release time in the event of 18 June 2000 (Figure 1a) was found to be 01:57 UT ± 6 minutes with the apparent path length of (1.80 ± 0.13) AU. In the event of 11 April 2004 (Figure 1b) the release time and the path length were 04:42 UT ± 2 minutes and (1.28 ± 0.05) AU. The onset times of the associated decametric type III and m and DH type II radio bursts are also marked in Figure 1a and b. It is seen that in the event of 18 June 2000 the proton release time is close to the onsets of the type III and DH type II bursts. In the event of 11 April 2004 the proton release time is delayed with respect to the radio emission onsets.

3.2. Electron Events Temporally Related to the Proton Events

We also performed VDA for the electron events associated with the 58 proton events. The onset times of electrons in the seven energy channels of the 3DP instrument were determined as described in Section 2. By using the same criterion for the apparent path lengths as for protons, we found 36 electron events temporally related to the selected proton events. The average apparent path length of electrons and the standard error in the 36 events were (1.58 ± 0.08) AU. The path length distributions had a maximum in the range 1.1 – 1.2 AU, close to the Parker spiral length. The electron path length distribution had a second maximum in the range 1.5 – 1.6 AU. The VDA results of the 36 electron events are summarized in Table 3 in the Appendix. The numbering of the events in Table 3 is the same as used in Table 2.
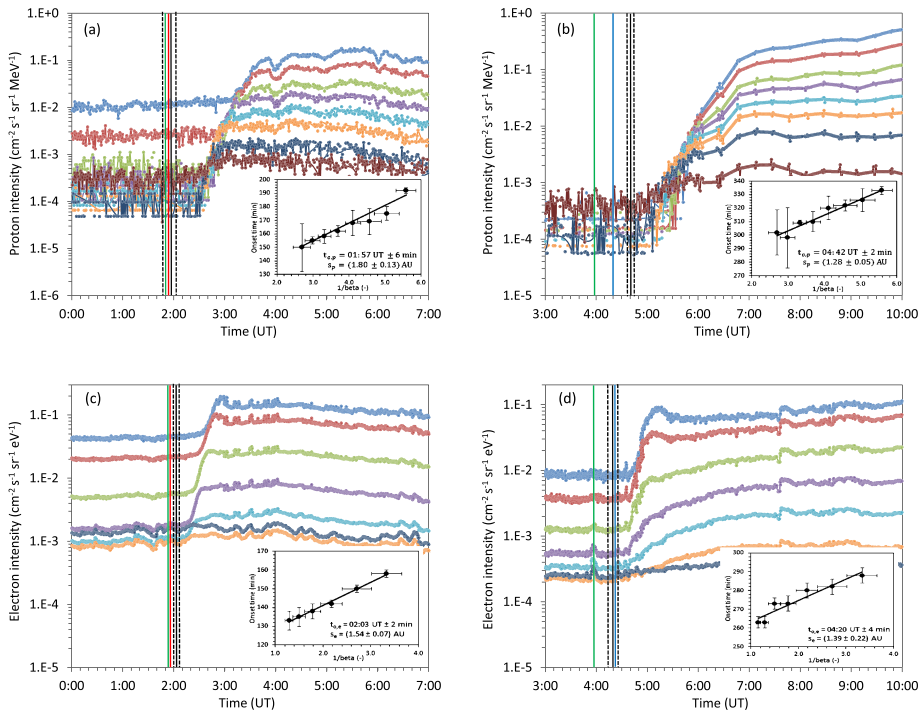
Figure 1 (**a**) The time–intensity profiles of protons in eight energy channels of ERNE in the event of 18 June 2000 and (**b**) the event of 11 April 2004. The ranges of the energy channels and their nominal energies from top to bottom are $(13.8-16.9)$ 15.4, $(16.9-22.4)$ 18.9, $(20.8-28.0)$ 23.3, $(25.9-32.2)$ 29.1, $(32.2-40.5)$ 36.4, $(40.5-50.8)$ 45.6, $(50.8-67.3)$ 57.4, and $(63.8-80.2)$ 72.0 MeV. (**c**) and (**d**) The time–intensity profiles of electrons in seven energy channels of *Wind*/3DP in the same events as for protons. The energy ranges and nominal energies from top to bottom are $(20-30)$ 27, $(30-50)$ 41, $(50-82)$ 86, $(82-135)$ 110, $(135-230)$ 180, $(230-392)$ 310, and $(392-646)$ 520 keV. The *solid* and *dashed black vertical lines* indicate the release times of protons and electrons and their uncertainties. The *green*, *red*, and *blue vertical lines* show the onset times of the decametric type III, metric type II, and decametric–hectometric type II radio emissions, respectively. In the inserted plots are the linear fits of the onset times (*black solid circles*) as a function of the reciprocal speed of the particles. The slopes of the fit lines and the interceptions with the ordinate axes (time from the beginning of the day in minutes) yield the given release times and apparent path lengths of the particles.

The time–intensity profiles and the VDA results for electrons in the events of 18 June 2000 and 11 April 2004 are presented in Figure 1c and d. For the event of 18 June 2000 we obtained the electron release time at 02:03 UT $\pm$ 2 minutes and the path length of (1.54 ± 0.07) AU. The corresponding values in the event of 11 April 2004 were 04:20 UT $\pm$ 4 minutes and (1.39 ± 0.22) AU. We note that in the event of 18 June 2000 the proton and electron release times were equal within the error limits, while in the event of 11 April 2004 the proton release time was delayed by about 22 minutes relative to the electron release time.

3.3. Proton and Electron Release Times and Path Lengths

We define events in general as "simultaneous" if their release times overlap when the uncertainties are taken into account. Otherwise, they are defined as "delayed". The total uncer-

Figure 2 Distribution of the differences between the proton and electron release times for the simultaneous proton and electron events (*black*) and for the proton events delayed with respect to the electron events (*light gray*). The single event of delayed electrons with respect to protons is shown by the *white column*. Simultaneous events are defined as those for which the release times overlap when the uncertainties are taken into account. Otherwise, the events are delayed.
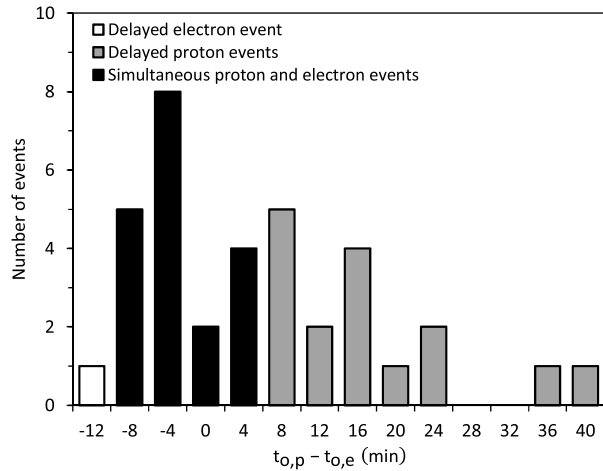
tainty for a pair of events is calculated simply by adding together the positive uncertainty of one event and the absolute value of the negative uncertainty of the other. For the particle release time uncertainties we use the standard deviations of the release times given by the fitting method used in VDA (see Section 2). The histograms presented in this and in the following sections are constructed using the nominal times (error margins not shown).

When comparing the release times of protons with those of the electrons in the 36 temporally related events, we found that with the exception of one event protons were released within the uncertainties simultaneously with or after the electrons. Only in one event (event 14) electrons were released after the protons. The distribution of the differences between the proton and electron release times is presented in Figure 2. The bin widths in Figure 2 are four minutes and each bin includes the events with the time differences greater than or equal to the bin value but smaller than the next larger bin value. The figure makes distinction between three groups: the simultaneous events for which the proton and electron release times are equal within the combined uncertainties of the particle release times given in Tables 2 and 3, and the delayed proton and the delayed electron events for which the proton and electron release times do not overlap in time within the uncertainties. Nineteen out of the 36 events (53%) are simultaneous events. The range of the release time differences for these events was from -6 to $+7$ minutes, with an average of -1 minutes. Of the rest, 17 events, 16 are delayed proton events and one delayed electron event. For the delayed proton events the release time differences of protons and electrons were from $+9$ to $+42$ minutes with an average of 18 minutes. For the single delayed electron event the difference was -10 minutes.

When comparing the path lengths of protons with those of electrons in the 36 temporally related events, we found that in 21 events the path lengths of protons and electrons overlapped within the uncertainties. The distribution of the proton and electron path length differences had a maximum at zero, but was skewed towards negative values. For the simultaneous events the average path lengths of protons and electrons were (1.51 ± 0.06) AU and (1.51 ± 0.11) AU, respectively. In the group of delayed proton events there was a significant difference between protons and electrons. Protons had a short average path length of (1.25 ± 0.06) AU, whereas the path length of electrons was longer, (1.65 ± 0.13) AU, but within uncertainties the same as in simultaneous events.

4. Radio Emission

The onset times of radio emissions (type II, III, and IV bursts) are defined here as the times of first appearance in the available dynamic radio spectra. For simplicity, we define DH emission to occur below the instrumental limit of space observations, while metric emission continues down to the lowest observable frequency of ground-based observations. In the events where the metric bursts appear to continue to DH wavelengths, we list them as both metric and DH bursts, and the onset times are those of the first appearance within the observed frequency ranges. As the ground-based observations come from different observatories that work in different time zones, there may have been gaps both in the observations and in the available frequency ranges. As several of our events originated near or behind the solar limb, the start of radio emission may have been blocked by the solar disc and the high-density solar corona. The radio burst onset times should therefore be interpreted as the latest possible (observed) start times.

In particular, we define the start time of decametric type III burst as the time when it is first observed at the highest frequency (usually at 14 MHz) in *Wind*/WAVES RAD2. Typically type IIIs occur in groups, and then the end time of the burst is taken as the latest time when the frequency of the last type III burst of the group reaches 1 MHz in RAD2. Only intense type III bursts and burst groups that were associated with the main flare are listed, and single faint type III bursts were discarded.

We define a radio burst to be associated with a proton event if the radio onset time is after the CME-associated flare start. In cases where we do not have a listed flare, which typically happens when the flare originates from an active region behind the limb, we use the estimated CME launch time as the time limit. In cases where there are multiple flares and CMEs propagating at the same time, the association may be uncertain. This applies especially to type II bursts, as they are known to originate from shocks at CME leading fronts and also from shocks at CME flanks at much lower heights. Therefore the estimated radio source heights may match with more than one CME.

4.1. Radio Type III Bursts

All the 58 proton events under study were estimated to be associated with decametric type III bursts observed by *Wind*/WAVES, but for three of the type III bursts we could not determine a reliable start time. These three bursts were associated with behind-the-limb events (events 21, 31, and 54) and the decametric emission started at very low frequencies, which indicates that the start of emission was blocked by the solar disk and atmosphere. We have therefore omitted these three events from the timing analysis. Taking into account the uncertainties in the proton release times, we found that in all but one event (event 14) protons were released at or after the type III onset. In 35 of the 55 events (64%) proton release occurred during the type III emission and in 19 events after the type III burst had ended.

4.2. Radio Type II Bursts

Fifty-six of the 58 proton events were associated with radio type II bursts: 11 events with m type II only, 11 with DH type II only, and 34 with type II radio bursts at both wavelength ranges. Only two events (events 4 and 35) occurred without any type II associations. When analyzing the differences between proton release times and type II onsets at m and DH wavelength ranges, we found that in two cases (events 19 and 32) protons were released before m type II emission, while in the remaining 43 events associated with m type II, protons were released at or after the m type II onset when uncertainties in the proton release

Figure 3 Difference between the proton release times and the decametric type III onset times as a function of the difference between the proton release times and the DH type II onset times for proton events associated with both m and DH type II bursts. The uncertainties of the data points are those of the proton release times. The *shaded area* represents the estimated average uncertainty in the onset times of the DH type II bursts associated with the six events shown with the *open diamonds* (see text for details).
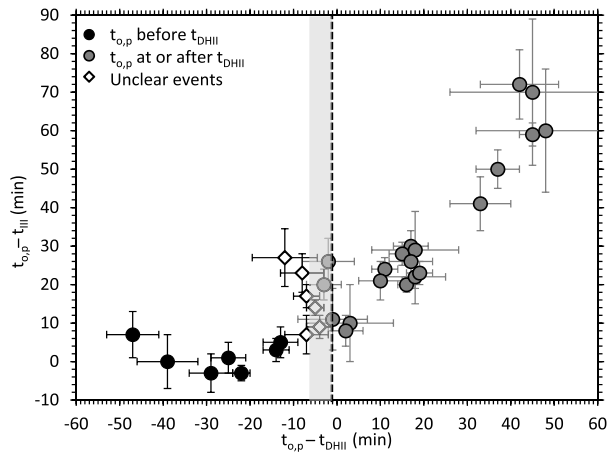
times were taken into account. In 31 of the 45 proton events associated with DH type II emission, protons were released at or after the DH type II onset. In eight events protons were released clearly before the DH type II onset, and in six events the onset of the DH type II burst was very close to the proton release time (see discussion in Section 4.4).

4.3. Radio Type IV Bursts

We did not find any DH type IV bursts associated with our 58 events, while 32 m type IV bursts were found. The absence of DH type IVs can be explained, at least partially, with the observed directivity of type IV bursts: in events where the burst source (flare) is located near or behind the solar limb DH type IV bursts are not observed (Gopalswamy *et al.*, 2016a; Talebpour Sheshvan and Pohjolainen, 2018). As m type IV bursts are thought to be formed by particles trapped in rising flare loops, their existence in intense and large soft X-ray flares can be considered as typical. As DH type IV bursts are thought to be formed by particles trapped in expanding CME loops, it may also be that the synchrotron emission does not exceed the plasma emission level and hence the type IV emission stays or becomes unobservable. In Table 2 we list two events for which we did not find m type IV associations from our data sources, but for which such associations are reported elsewhere. We treated these associations as uncertain (marked as "Yes?"), and did not include these events in m type IV related analyses. In 25 of the events for which associated m type IV emission was observed, the proton release time was within the duration of the type IV burst. In three cases the proton release time was before the type IV burst onset and in three cases after it had ended. In one case the end of the m type IV burst remained unknown.

4.4. Proton Event Categories Based on Radio Type II Bursts

Proton release times show regular behavior with respect to the radio emission onset times. This is demonstrated in Figure 3, where we present the difference between the proton release times and the type III onset times as a function of the difference between the release times and the DH type II onsets for those events, which were associated with both m and DH type II bursts. In Figure 3, the filled black circles are the events with the proton release times before DH type II onsets and the filled gray circles the events with the release times at or after the DH type II onsets within uncertainties. In six cases (open diamonds in Figure 3), the

proton release time was before, but within uncertainties very close to the DH type II onset. The average estimated uncertainty in the onset times of the DH type II bursts associated with these six events is presented in Figure 3 with the shaded rectangle to the left from the zero time difference (dashed vertical line). In event 58 the proton release time was very early (-77 minutes; not shown in Figure 3) compared to the DH type II onset. We considered the DH type II association in this event uncertain and discarded the event from further analysis.

We investigated several properties of the proton events (see Section 5 and Table 1) and discovered that the events can be divided into two broad categories based on the type II burst wavelength range and on the temporal relation between the proton release times and the type II onsets. Events belonging to the same category had similar properties, while the properties of events in different categories were significantly different. Category 1 consists of the events which are associated with only m type II emission or both m and DH type II and the release time of protons is before the DH type II onset (18/56 events). In Category 2 are the events which are associated with only DH type II emission or both m and DH type II and the proton release time is at or after the DH type II onset (31/56 events). Thus, in Figure 3 the events shown with the black circles belong to Category 1, and those shown with the gray circles belong to Category 2. For the six events shown in Figure 3 with the open diamonds only minor changes in the estimated total time uncertainties were critical in determining the category which these events belonged to. We considered the exact category of these events (events 8, 12, 24, 40, 43, and 52) unclear and in order to keep the categories distinctly separate, we decided not to include these events in further analysis.

The distributions of the time differences between the proton release times and the type III, type m II, type DH II, and type m IV radio onsets for Category 1 and Category 2 events are presented in Figure 4. On average Category 1 events have clearly smaller differences $t_{o,p} - t_{\mathrm{III}}$ and $t_{o,p} - t_{\mathrm{mII}}$ than category 2 events (Figure 4a and b). In almost all Category 1 events (15/18) proton release occurred during the type III emission. The bin -10 minutes in Figure 4a includes two events for which the differences between the nominal proton release times and the type III onsets were negative (events 14 and 29), but within the uncertainties protons were released before the type III onset only in event 14. Similarly, in Figure 4b only in event 32 in the bin -20 minutes and in one of the events in the bin -10 minutes (event 19) protons were released before m type II onset. By definition the differences $t_{o,p} - t_{\mathrm{DHII}}$ are distinctly separate for the events in the two categories (Figure 4c). Although there are three Category 2 events in the bin -10 minutes in Figure 4c, these events (gray circles in the shaded area in Figure 3) have proton release times within uncertainties simultaneously with the DH type II onsets. The distributions of $t_{o,p} - t_{\mathrm{mIV}}$ are less distinct between the categories (Figure 4d), but clearly the Category 2 events are concentrated in larger time differences than Category 1 events. In only two Category 1 events protons were released within uncertainties after the m type IV onset, whereas this was the case for all but one Category 2 events.

4.5. Proton Events and Temporally Related Electron Events

Based on the release time differences of protons and electrons in the temporally related 36 events, we defined in Section 3.3 simultaneous proton and electron events and delayed proton events and found also one event in which electrons were released after protons (Figure 2). The temporal relations of these groups with respect to decametric type III bursts are presented in Figure 5. Figure 5a shows the differences between the electron release times and type III onset times as a function of the differences between the proton release times and type III onset times. The groups of simultaneous proton and electron events and the delayed proton events are clearly distinct. In several events there is a significant time difference (> 20 minutes) between the electron release time and the type III onset. For simultaneous
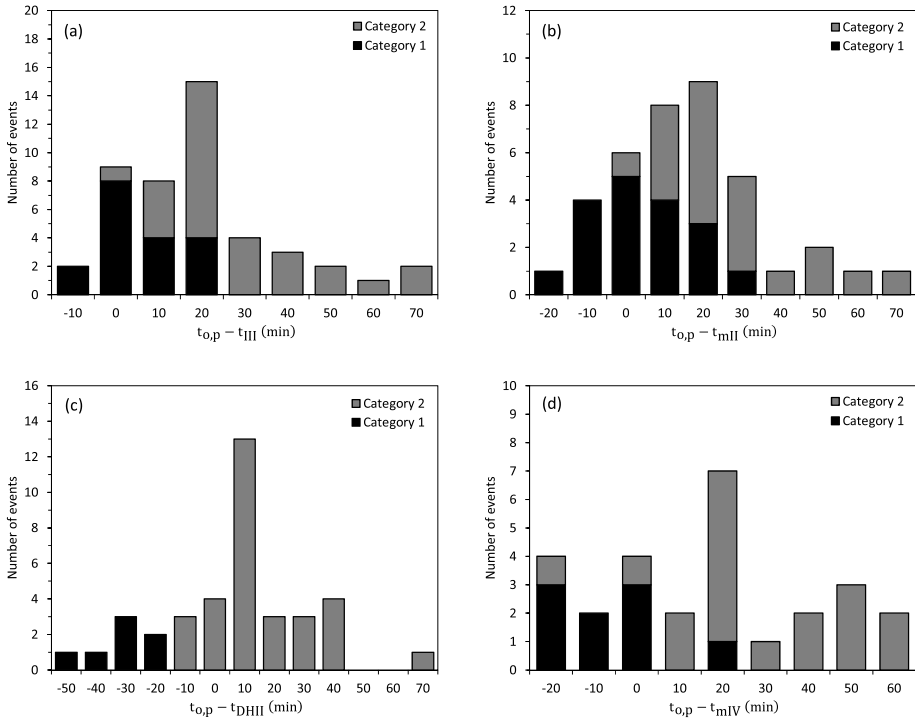
Figure 4 (**a**) Distributions of the differences between the proton release times and the associated decametric type III onsets for Category 1 and Category 2 events. (**b**) and (**c**) Distributions of the differences between the proton release times and the metric and decametric–hectometric type II onsets. (**d**) Distributions of the differences between the proton release times and the associated metric type IV onsets.
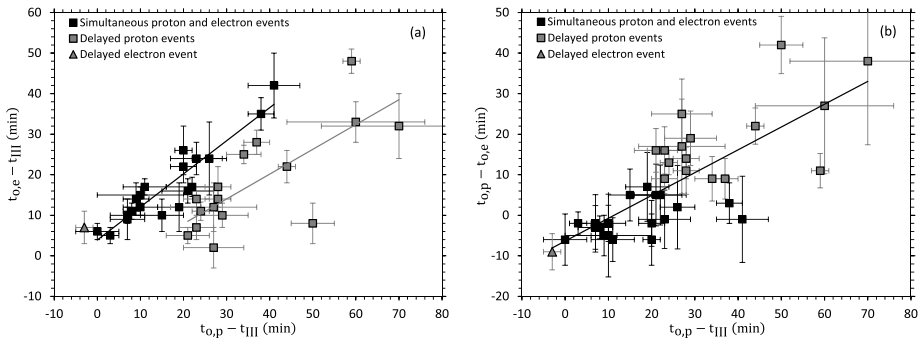

Figure 5 (**a**) Scatter plot of the differences between the electron release times and the associated decametric type III onsets as a function of the differences between the proton release times and the decametric type III onsets for the simultaneous proton and electron events and for the delayed events. (**b**) As (**a**), but for the differences between the proton and electron release times. Linear fits to the data are included to guide the eye.

events, for which the release times of protons and electrons are close to each other, the difference $t_{o,e} - t_{III}$ correlates well with $t_{o,p} - t_{III}$. The correlation coefficient is $r = 0.83 \pm 0.06$. Here and in what follows, all Pearson correlation coefficients given have been calculated

taking into account the uncertainties in the data. This was done by randomly selecting each data point from a Gaussian distribution having the most probable value equal to the nominal value of the data point and the standard deviation equal to the uncertainty of the data point. The procedure was repeated 10 000 times and for each iteration the correlation coefficient was calculated using the inverse squares of the total uncertainties as weights. The average of the 10 000 iterations and their standard deviation is given as the correlation coefficient.

In Figure 5a the delayed proton events form a group separate from the simultaneous events. The differences $t_{o,e} - t_{III}$ are similar to the simultaneous events, but the differences $t_{o,p} - t_{III}$ are larger. In these events the proton release times are not only later than those of the electrons, but the proton release is also more delayed with respect to decametric type III emission. The dependence between the time differences is not as strong as for the simultaneous events, and at $t_{o,p} - t_{III}$ above about 35 minutes the values are widely scattered. In 16 of the 19 (84%) simultaneous events, the proton release occurred during the type III emission, while in 12 of the 16 (75%) delayed proton events protons were released after the type III burst had ended. For electrons no such trend was observed, but in roughly 80% of the events in both groups electrons were released during the type III emission.

In relation to type m IV emission, the simultaneous proton and electron events and the delayed proton events were similar: about half of the events in both groups had an associated m type IV burst (11/19 in simultaneous events and 7/16 in delayed proton events). In the group of simultaneous events electrons were always released during the m type IV emission. The same was true for protons excluding one event in which protons were released after the m type IV burst had ended. In the group of delayed proton events, both electrons and protons were released before the m type IV onset in one event, in one event protons were released after the end of type IV burst, and in the rest of the events the particles were released during the m type IV emission. In the single event of delayed electron release with respect to protons, both particle species were released during the m type IV emission.

Figure 5b shows the differences between the proton and electron release times as a function of the differences between the proton release times and type III onset times for the simultaneous and delayed events. The event groups are again well separable, the simultaneous events having generally smaller time differences than the delayed proton events in both variables. The general trend visible in Figure 5b is that the difference between the proton and electron release times increases with the increasing difference between the proton release time and the type III onset time.

In the group of simultaneous proton and electron events there was no clear division of the events into Categories 1 and 2. Six simultaneous events belonged to Category 1 and nine in Category 2. For three events the category was unclear and one was not associated with type II emission. In the group of delayed proton events, the distinction was more pronounced: only two events belonged to Category 1 and 11 to Category 2. For two events the category was unclear and one was not associated with type II emission. All the simultaneous and delayed proton events belonging to Category 1 were associated with only m type II emission. The single delayed electron event belonged to Category 1, and it was the only proton event with a temporally related electron event in this category which was associated with both m and DH type II emission.

5. Properties of High Energy Proton Events

5.1. Release Times and Solar Source Locations

We studied the dependence of the time differences between the proton release times and the decametric type III radio burst onset times on the solar source locations of the particle
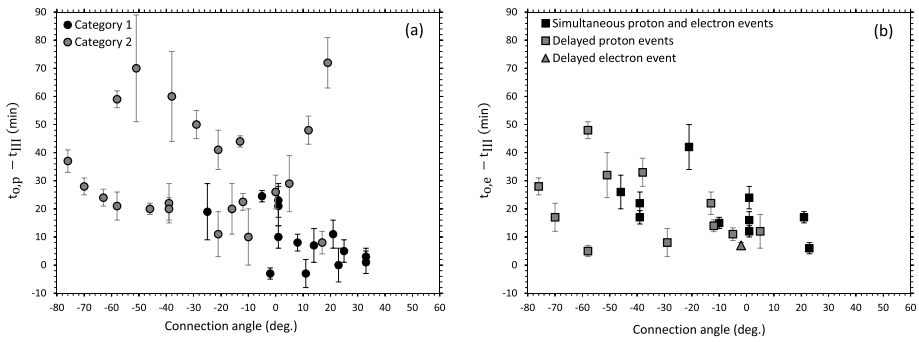
Figure 6 (**a**) Scatter plot of the differences between the proton release times and the associated decametric type III onsets as a function of the connection angle for Category 1 and Category 2 events. The connection angle is defined as positive, when the flare location is to the west from the magnetic footpoint of the Parker spiral leading to Earth. (**b**) Differences between the electron release times and the associated decametric type III onsets as a function of the connection angle for those simultaneous and delayed events which belong to Categories 1 or 2. For clarity, the connection angle error bars are neglected.

events, which were assumed to coincide with the flare locations. We performed this study both for the longitudinal distance $\Delta\phi$ of the flare from the footpoint of the Parker spiral leading to the spacecraft near 1 AU and simply for the flare longitude. The longitudinal distance (connection angle) was calculated as

$$\Delta\phi = \phi_{\mathrm{fl}} - \frac{\Omega_{\odot} r_{s/c}}{u_{\mathrm{sw}}}, \tag{2}$$

where ϕ_{fl} is the solar flare longitude, $2\pi\Omega_{\odot}^{-1} = 24.47d$ is the equatorial period of the solar rotation, $r_{s/c}$ is the radial distance of the spacecraft from the Sun, and u_{sw} is the average solar wind speed at the time of the SEP event onset observed by the SOHO spacecraft. The solar wind speed was averaged over the period of seven hours centered at the hour of the proton release time. The longitudinal distance of the footpoint from the flare location is positive, if the flare is to the west from the footpoint and negative if the flare is to the east. The derived connection angles are given in Table 2 in the Appendix.

This study concentrated in total 41 proton events for which the definite flare locations were known. Fourteen of these belonged to Category 1 and 22 to Category 2. The results for the two categories are presented in Figure 6a. The vertical error bars in Figure 6a are the uncertainties of the proton release times. We estimated the uncertainties in the type III onset times to be insignificant compared to the uncertainties in the particle release times, and they are neglected. Uncertainties in the connection angles can also be of the order of $\pm 10°$ (*e.g.* Klein *et al.*, 2008). However, since these error bars do not change the general picture in Figure 6, they are omitted for clarity. All Category 1 events have small connection angles roughly in the range $[-25°, +35°]$, most of them close zero or at positive angles. They also have small differences between proton release times and type III onsets between 0 and 20 minutes. Category 2 events are more scattered both in connection angle and in $t_{o,p} - t_{\mathrm{III}}$, but many have large negative connection angles and time differences mainly above 20 minutes with no correlation between the time difference and the connection angle ($r = -0.002 \pm 0.091$). In the calculation of the coefficient, $\pm 10°$ uncertainties were taken into account in the connection angles. Overall, the range of connection angles of Category 2 events extends from $+19°$ down to $-76°$. There is only a weak dependence between the

time difference and connection angle for all events taken together ($r = -0.41 \pm 0.06$), although the average values of the connection angles for Category 1 and Category 2 events are significantly different.

In Section 5.5 we describe some properties of the soft X-ray flares associated with Category 1 and Category 2 proton events, but it is appropriate to note here that our data set showed no evidence that events with large connection angles would be associated with flares of higher magnitude than those with small connection angles (Miteva *et al.*, 2013). Eleven proton events under study were associated with X-class flares. Two of these occurred at connection angles $< -30°$, one at connection angle $> +30°$, three in the range $[-30°, 0°]$, and five in the range $(0°, +30°]$. Therefore, connection angle-dependent strong-flare association does not play a role in the results.

Altogether 22 Category 1 and Category 2 events had temporally related electron events, and for these events we also made distinction between the simultaneous proton and electron events and the delayed events. Figure 6b is similar to Figure 6a, but for the simultaneous and delayed events and for the time difference between the electron release time and the type III onset. This time difference is less scattered than using the proton release time, but there is no clear dependence on the connection angle nor very large difference between the groups of the simultaneous and delayed proton events. Several of the delayed proton events (5/11) have small connection angles in the range $[-29°, +5°]$. At least in these cases protons should have quite easily reached open magnetic field lines (if they existed) connecting to the observation point near Earth. Most of the simultaneous proton and electron events (7/10) have small connection angles, but there are also three exceptions with relatively large negative angles. The one event with electron release time later than proton release time (gray triangle in Figure 6b) is close to zero connection angle and zero time difference $t_{o,p} - t_{\mathrm{III}}$.

The dependence of $t_{o,p} - t_{\mathrm{III}}$ on the source longitude showed similar behavior as on the connection angle. With the exception of one event, all Category 1 events had source locations between longitudes 52W and 85W, in the magnetically well-connected region. Category 2 events were quite evenly distributed in the the western hemisphere with three events at eastern longitudes. It is noteworthy, however, that while only three Category 1 events had a negative connection angle, for all but five Category 2 events the connection angle was negative (Figure 6a). There was no significant difference in the longitude distributions of the simultaneous electron and proton events and the delayed proton events, although the simultaneous events were more concentrated in western longitudes.

5.2. Proton Release and Shock Formation Heights

If protons are accelerated in CME-driven shocks (see *e.g.* Reames, 1999), then with certain assumptions and approximations the release heights of protons can be estimated from CME heights. We used the height–time data from the SOHO/LASCO CME catalog for the CMEs related to 56 SEP events. For two events of our list the SOHO/LASCO data were not available. We assumed constant speeds of the CMEs and extrapolated the heights downwards, when necessary, using a linear fit to the available height–time data. We further assumed that the release height of protons was the height at which the leading front of the CME was at the proton release time as obtained from the velocity dispersion analysis (Section 3 and Table 2). When using this method, we assume that the acceleration takes place in a shock close to the leading front of a CME. Thus, there may be considerable uncertainties in the derived heights on one hand because particles can be released anywhere between the CME front and the shock front and on the other hand because shocks can also occur on the flanks of the CMEs. Extrapolation of the height–time data downwards assuming a constant speed for the CMEs can cause errors in the derived heights as well.
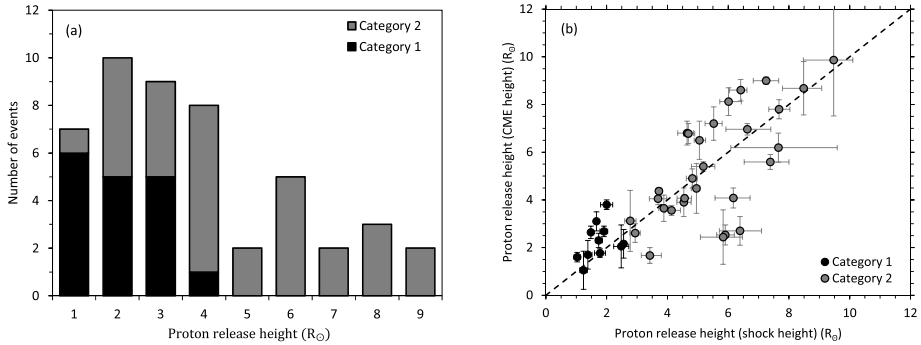
Figure 7 (**a**) Distribution of the estimated proton release heights for Category 1 and Category 2 events based on the CME height–time data. (**b**) Scatter plot of the proton release heights estimated from the type II burst (shock) heights, calculated using an atmospheric density model, and the corresponding CME leading front heights. Heights below 2.6 $R_\odot$ were derived from the dynamic spectra in the meter wavelength range, which is associated with Category 1 events. Category 2 events are associated with the DH wavelength range, which was used to derive the heights above 2.7 $R_\odot$. The *dashed line* represents equal values from the two methods.

A histogram of the proton release heights of the events belonging to the two categories is presented in Figure 7a. The range of Category 1 release heights is from 1.1 to 4.4 $R_\odot$ with all but one event in the bins $1-3$ $R_\odot$. The Category 1 event in bin 4 $R_\odot$ is the delayed electron event. The range of Category 2 events is from 1.7 to 9.9 $R_\odot$ with only one event in the bin 1 $R_\odot$ and a maximum at 4 $R_\odot$. The averages with standard errors are (2.6 ± 0.2) $R_\odot$ and (5.2 ± 0.4) $R_\odot$ for Category 1 and Category 2 events, respectively.

With the aim to verify the release height results by an independent method, we used the radio type II observations to deduce the shock heights. We determined the type II burst frequencies at the time of the proton release, and then used the atmospheric electron density model of Vršnak, Magdalenić, and Zlobec ([2004](#)) to calculate the shock heights at those times. The hybrid density model of Vršnak, Magdalenić, and Zlobec ([2004](#)) merges the high-density low-corona models with the low-density IP models without discontinuities. It is basically a mixture of the five-fold Saito model (Saito *et al.*, [1970](#)) and the model of Leblanc, Dulk, and Bougeret ([1998](#)) with small modifications. We assume that the proton release height coincides with the shock height at the release time. We determined the frequencies by eye at the center of either fundamental or harmonic lane and estimated the uncertainties as the width of the lane.

It was possible to estimate the shock height at the time of the proton release for 41 of the 49 Category 1 and Category 2 events. The main reason for unsuccessful shock height determination was that no type II lane was visible in the dynamic spectra at the time of the proton release. In two Category 1 events the proton release time was before the m type II onset and in one Category 2 event after the end of the DH type II. Altogether, the shock heights were obtained for 12 Category 1 and 29 Category 2 events. The shock heights at the time of the proton release varied from 1.1 to 9.5 $R_\odot$ with the heights below 2.6 $R_\odot$ derived from the dynamic spectra in the meter wavelength range and above 2.7 $R_\odot$ from the dynamic spectra in the decameter–hectometer wavelength range.

Figure 7b compares the proton release heights obtained from the CME heights and from the shock heights for Category 1 and Category 2 proton events. The uncertainties in the shock heights represent the inaccuracy in determining the type II frequencies at the proton release times, and those in the CME heights take into account the uncertainties in the proton release times. The dashed line depicts equal values from the two methods. In general,

the data points follow this line, the two methods giving equal release heights within the uncertainties in about half of the events. CME heights above the dashed line may be due to the shock not having formed on the CME front, but somewhere on the flank. There are also a few events with clearly higher values of shock heights than CME heights. Reasons for these discrepancies may be an incorrect identification of the type II lane in the case of multiple shocks or an incorrect association of a shock with a CME in the case of multiple CMEs. Also, using extrapolation of the CME height–time data below the coronagraph field of view can lead to significant errors in the CME height. Figure 7b, however, clearly shows that based on the shock heights, all Category 1 events are released at heights below 2.6 $R_\odot$, while the Category 2 events are released higher in the solar corona. The shock heights thus give a clearer picture of the proton release heights within the two categories than the CME heights (Figure 7a).

As described in Section 4.5, there was no clear division of the simultaneous proton and electron events and the delayed proton events into Categories 1 and 2. The simultaneous and the delayed events did not show a corresponding systematic behavior as Category 1 and Category 2 events in Figure 7. For the simultaneous events the release heights of protons obtained from the shock heights ranged from 1.1 to 8.5 $R_\odot$, but concentrated (71% of the events) below 5.0 $R_\odot$. For the delayed proton events the range was from 3.4 to 9.5 $R_\odot$. In the single delayed electron event the proton release height given by the shock height was 1.8 $R_\odot$.

It is well known that the time difference between shock formation and particle release is of the order of 10 minutes (Gopalswamy *et al.*, 2016b, and the references therein). Taking the onset time of the type II emission as the shock formation time we found that for all of our events taken together the average time difference was (21 ± 3) minutes with a clear difference between Category 1 ((9 ± 3) minutes) and Category 2 ((29 ± 4) minutes) events. We determined the shock formation heights based on the starting frequency of type II emission and using the hybrid density model or the empirical formula relating the type II starting frequency to the shock formation height given by Gopalswamy *et al.* (2013). The two methods gave consistent average values of (1.32 ± 0.04) $R_\odot$ and (1.34 ± 0.04) $R_\odot$ for Category 1 events and (2.0 ± 0.2) $R_\odot$ and (1.8 ± 0.1) $R_\odot$ for Category 2 events. These shock formation heights are different at $> 99\%$ confidence level for Category 1 and Category 2 events.

5.3. Proton Time-Intensity Profiles

We analyzed the time–intensity profiles of protons at the rise phase of the events in the energy channel $50.8 - 67.4$ MeV. We first determined the background intensity, I_{bg}, of each event in the time window of one hour before the onset, and subtracted the logarithm of this intensity from the logarithm of the observed intensity during the event. We defined the rise rate of an event as the difference between the logarithms of the background-normalized intensities at 80% and 20% of the maximum divided by the corresponding rise time,

$$\frac{\Delta(\log I)}{\Delta t} = \frac{0.8 \log[I_{max}/I_{bg}] - 0.2 \log[I_{max}/I_{bg}]}{t_{0.8} - t_{0.2}}, \tag{3}$$

where $t_{0.2}$ and $t_{0.8}$ are the times when the background-normalized intensity reached 20% and 80% of its maximum value. The maximum intensity was selected from close to the end of the main rise phase of the event to avoid possible small fluctuations and peaks from energetic storm particles late during the event. The rise rates for the 58 proton events ranged from 0.0037 min^{-1} to 0.21 min^{-1}.
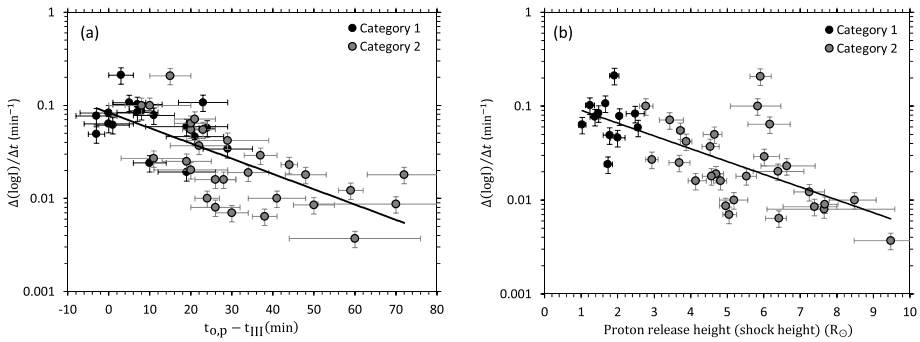
Figure 8 (**a**) Scatter plot of the proton intensity rise rates as a function of the differences between the proton release times and the associated decametric type III onset times. (**b**) The same as (**a**), but as a function of the proton release height obtained as the shock height. Linear fits to the data are included to guide the eye.

The rise rates for the Category 1 and Category 2 proton events are presented in Figure 8a as a function of the differences between the proton release times and the decametric type III radio onsets and in Figure 8b as a function of the proton release height obtained as the shock height at the time of the proton release. The main sources of uncertainty in the rise rates are the level of the background intensity and the selected maximum intensity. Using the 20% and 80% limits of the normalized intensities minimizes the rise rate uncertainties, and they are estimated to be at maximum 20%, which are shown in Figure 8. The rise rates of the proton intensities are clearly decreasing with increasing differences between the proton release times and the decametric type III onsets as well as with the increasing release heights. As already shown in Figure 4a, Category 1 events have in general lower time differences $t_{o,p} - t_{III}$ than Category 2 events, and Figure 8a shows that they also have in general higher intensity rise rates. Several of the Category 2 events, which have comparable time differences with Category 1 events also have comparable rise rates, but at larger time differences the rise rates are significantly lower. When the proton release height obtained as the shock height is used as the independent variable, the distinction between Category 1 and Category 2 events is clear (Figure 8b). In Category 1 events the protons are released at low heights below 2.5 $R_\odot$ (see also Figure 7b) and have high rise rates. Category 2 events have generally lower rise rates and large release heights. Overall, the decreasing intensity rise rates correlate well with increasing release heights with a correlation coefficient of -0.78 ± 0.02.

In a presentation corresponding to Figure 8a, the rise rates of proton intensities in the simultaneous proton and electron events and in the delayed proton events showed a similar behavior as Category 1 and Category 2 events. The time differences $t_{o,p} - t_{III}$ were larger in the delayed events and the rise rates were generally lower than in the simultaneous events. Because there was no clear distinction in the release heights of the simultaneous and delayed proton events, these two groups did not show a clear difference in the rise rates as a function of the release heights, although in general the rise rates were decreasing with increasing release heights.

5.4. Proton Energy Spectra

We constructed single-power-law energy spectra for the Category 1 and Category 2 proton events in the energy range $13 - 80$ MeV. We calculated the spectra from the background-subtracted intensities at the time of the maximum intensity using 1-hour integration time

Figure 9 Power-law spectral indices of protons for Category 1 and Category 2 events as a function of the release height.
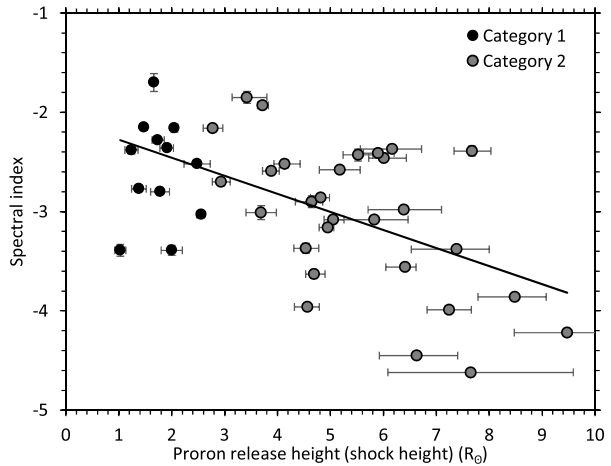
in most cases. For some events we used shorter integration times due to a rapid fall of the intensities after maximum, in particular at the highest energies. We derived the spectral indices from the intensity *vs.* energy data in the log–log scale by using the same fitting method as for the VDA (see Section 3). As the intensity uncertainties we used the combinations of the statistical uncertainties and the standard deviations of the 1-minute average intensities during the integration times. The energy channel widths were used as the uncertainties for the energies.

The spectral indices for Category 1 and Category 2 events are presented in Figure 9 as a function of the proton release height based on the shock height at the time of the proton release. The spectral indices for Category 1 events varied from -1.7 to -3.4 and for Category 2 events from -1.9 to -4.6. Thus, there is a quite significant overlap of the spectral indices in the two categories, but many of the Category 2 events also have lower indices than Category 1 events. The overall decrease of the spectral indices, *i.e.* softening of the spectra, with increasing release height is clear.

A corresponding dependence of spectral indices as a function of the proton release height as shown for Category 1 and Category 2 events in Figure 9 was not observed for the simultaneous proton and electron events or for the delayed proton events.

5.5. Soft X-Rays and Coronal Mass Ejections Associated with Proton Events

Soft X-ray onset times, peak times, and end times were available for 17 Category 1 and for 26 Category 2 proton events. For one Category 2 event (event 53) a very long rise time of 312 minutes was reported. In all other events, the rise times ranged from 3 minutes to 68 minutes. Due to the significant deviation from the other events, this event was excluded from the comparisons of the characteristics of the X-ray flares between the two categories. We found a significant difference in the average rise time and duration of the flares associated with the Category 1 and Category 2 events, while the average peak flux did not significantly differ. The average rise time and duration of the flares in Category 1 events were (14 ± 2) minutes and (24 ± 4) minutes, respectively, while in Category 2 events they were (27 ± 3) minutes and (54 ± 6) minutes. We also found that in 11 of the 17 (65%) Category 1 events, the proton release time was before or within uncertainties coincident with the X-ray peak time, while in 20 of the 26 (77%) Category 2 events it was after the X-ray peak time.

X-ray time information was available for 15 of the 19 simultaneous proton and electron events and for 15 of the 16 delayed proton events. In all delayed proton events the protons were released after the X-ray peak time. The same was true for nine of the 15 simultaneous proton and electron events, while in the rest the release was before the X-ray peak time or coincident within the timing uncertainties. In the single event in which the electrons were released later than protons, the protons were released before the X-ray peak time.

There were no significant differences in the average CME (sky-plane) speed in either between the Category 1 and Category 2 events or the simultaneous and delayed electron and proton events, whereas the CME average width in Category 2 events was larger than in Category 1 events. The differences in the CME speed and width were more significant when events with only m type II association in Category 1 and with only DH type II association in Category 2 were compared: for these restricted sets of events both the CME speed and the width in Category 2 events were clearly larger than in Category 1 events.

We also estimated the CME initial acceleration defined as the CME space speed divided by the soft X-ray flare rise time (Zhang *et al.*, 2001; Zhang and Dere, 2006; Gopalswamy *et al.*, 2016b). For halo CMEs we used the space speeds given in the CDAW halo CME list (Gopalswamy *et al.*, 2010). The space speeds of non-halo CMEs (width $> 100°$) we estimated by using the cone model of Xie, Ofman, and Lawrence (2004) and the formula given by Gopalswamy *et al.* (2010). The range of the initial acceleration in Category 1 events was from $0.53 \ \mathrm{km\,s^{-2}}$ to $4.53 \ \mathrm{km\,s^{-2}}$ with most (75%) of the events below $2 \ \mathrm{km\,s^{-2}}$ and an average of $(1.7 \pm 0.3) \ \mathrm{km\,s^{-2}}$. In Category 2 the range was from $0.10 \ \mathrm{km\,s^{-2}}$ to $2.76 \ \mathrm{km\,s^{-2}}$ with 56% of the events below $1 \ \mathrm{km\,s^{-2}}$ and an average of $(1.1 \pm 0.2) \ \mathrm{km\,s^{-2}}$. The difference in the average initial CME acceleration in Category 1 and Category 2 events is not statistically significant (confidence level $< 90\%$).

6. Summary of the Results

We have investigated the dependence of the characteristics of 58 high-energy proton events on the associations of type II, III, and IV radio bursts. Proton events from the time period $1997 - 2015$ for which VDA gave a reasonable apparent path length of $1 - 3$ AU were selected for analysis. We also searched for and analyzed 36 near-relativistic electron events temporally related to the proton events and fulfilling the same path length criterion. Moreover, we examined the properties of soft X-ray flares and CMEs associated with the proton events.

We summarize our results as follows:

All proton events were associated with decametric type III emission, but for three events a reliable start time could not be determined. In 35 of the 55 events, protons were released during the type III burst, in one event before the type III onset and in 19 events after the type III burst had ended.

Almost all (56/58) proton events were associated with type II bursts: 11 with m type II only, 11 with DH type II only, and 34 with both m and DH type II.

Thirty-two of the events were associated with m type IV burst, whereas DH type IV was not associated with any of the events.

By examining several characteristics of the proton events we discovered that the events can be divided into two categories. The characteristics of events belonging to the same category were similar, while they significantly differed between events in different categories. The distinctive factors between the categories were the wavelength range of the associated type II radio emission and the temporal relation of the proton release with respect to the

Table 1 Average values with standard errors of properties of solar proton events in the two categories based on the associated radio type II burst wavelength range and on the proton release time with respect to the type II burst onset time.

Parameter	Category 1	Category 2	Confidence level[a]
Maximum intensity ($cm^{-2} s^{-1} sr^{-1} MeV^{-1}$)	0.13 ± 0.05	0.066 ± 0.023	< 95
Intensity rise rate (min^{-1})	0.075 ± 0.010	0.035 ± 0.007	> 99
Intensity rise time (h)	0.59 ± 0.08	2.4 ± 0.4	> 99
Release height ($R_\odot$)	1.8 ± 0.2	5.5 ± 0.3	> 99
Spectral index	-2.55 ± 0.13	-3.09 ± 0.13	> 99
$t_{o,p} - t_{III}$ (min)	10 ± 2	32 ± 3	> 99
$t_{o,e} - t_{III}$ (min)	13 ± 2	23 ± 3	> 98
$t_{o,p} - t_{o,e}$ (min)	1 ± 3	11 ± 3	> 95
Proton path length (AU)	1.50 ± 0.09	1.59 ± 0.08	< 95
Electron path length (AU)	1.31 ± 0.08	1.68 ± 0.12	< 95
Connection angle (°)	10 ± 4	-28 ± 6	> 99
Solar flare longitude (°)	62 ± 6	34 ± 6	> 99
Solar soft X-ray flare rise time (min)	14 ± 2	27 ± 3	> 99
Solar soft X-ray flare duration (min)	24 ± 4	54 ± 6	> 99
Solar soft X-ray flare peak flux (10^{-4} Wm^{-2})	2.3 ± 1.0	0.66 ± 0.15	< 95
CME speed ($km s^{-1}$)	1070 ± 130	1220 ± 90	< 95
CME angular width (°)	220 ± 30	300 ± 20	> 97
CME initial acceleration ($km s^{-2}$)	1.7 ± 0.3	1.1 ± 0.2	< 95
Delayed proton events	2/9 (22%)	11/20 (55%)	–

[a]Confidence level (%) at which the averages of the two categories are different.

type II onset. Category 1 consists of 18 events which are associated with only m type II emission or both m and DH type II and the release time of protons is before the DH type II onset. Category 2 includes 31 events which are associated with only DH type II emission or both m and DH type II and the proton release time is at or after the DH type II onset. For seven events designation of a definite category was unclear due to timing uncertainties and these events were not included in the analysis.

When investigating the 36 electron events temporally related to the proton events, we found that within timing uncertainties in 19 of the 36 events electrons were released simultaneously with the protons, in 16 events proton release was delayed with respect to the electrons, and in only one event electrons were released after the protons. The proton events in the groups of simultaneous and delayed events did not unambiguously fall into the two categories based on the type II associations. Only two delayed proton events and the single delayed electron event belonged to Category 1 together with five simultaneous proton and electron events, whereas in Category 2 there were almost equal numbers of simultaneous proton and electron events and delayed proton events.

The average values of several parameters describing the proton events in the two categories are summarized in Table 1. The given average proton release heights of Category 1 and Category 2 events are based on the shock height at the proton release time derived from the atmospheric density model. The corresponding values derived from the CME leading front heights were (2.6 ± 0.2) $R_\odot$ and (5.2 ± 0.4) $R_\odot$ for Category 1 and Category 2 events, respectively. The table also shows the confidence level at which the parameter values are

different between the two categories. The given confidence levels are based on Student's two-tailed t-test for two samples. Of the listed average parameter values, only the maximum intensity of the events, the path length of both protons and electrons, the peak flux of the associated X-ray flares, and the CME speed are not significantly different. Between the groups of simultaneous proton and electron events and the delayed proton events, the only significantly different (at $> 99\%$ confidence level) average parameter values were the difference between the proton release time and the type III onset, the difference between the proton and electron release times, and the path length of protons. In addition, within the group of delayed proton events there was a significant difference in the average path lengths of protons and electrons.

7. Discussion

Our investigation of the characteristics of high-energy solar proton events and their association and relative timing with respect to radio type II onsets led us to define two categories of proton events. On the other hand, when investigating the release times of the near-relativistic electron events temporally related to the proton events, we found that with only one exception protons were released within timing uncertainties simultaneously with or later than electrons.

7.1. Associations and Temporal Relations of Proton Events with Radio Emissions

In accordance with earlier studies (*e.g.* Cane, Erickson, and Prestage, 2002; Cliver and Ling, 2009; Xie *et al.*, 2016), all our 58 proton events were associated with decametric type III emission. All but two were associated with type II emission. Metric type II was associated with 45 events and DH type II also with 45 events. This is somewhat different from Xie *et al.* (2016), who report DH type II associations for all of their 28 events and m type II associations for 21 events. Thirty-two proton events were associated with m type IV bursts, whereas DH type IV association was not found for any event. Considering all events originating from the visible disk of the Sun, the characteristics of the proton events did not differ in events with m type IV association from those in which m type IV was absent. The differences in the characteristics of Category 1 and Category 2 events with and without m type IV associations were similar to those presented in Table 1.

The release times of protons with respect to the onsets of various types of radio emissions in the defined two categories were presented in Figure 4. It is clear that for Category 1 events the release times of protons are closer to the onset times of both decametric type III and m type II bursts compared to Category 2 events. Thus, the release of protons in Category 1 events is temporally more closely related to the flare processes producing the electron beams leading to radio type III emission and to the development of shocks low in the corona. In almost all Category 1 events (15/18) proton release occurred during the type III emission. In one event the derived proton release time taking into account the uncertainties was before the type III onset and in two events before the m type II onsets, while in Category 2 events the release times were generally clearly after the type III and m type II onsets. By definition, in all Category 2 events the proton release times were at or after the DH type II onsets.

7.2. Does Connection Angle Explain the Differences Between Category 1 and Category 2 Events?

It is well known that certain characteristics of SEP events are dependent on the solar longitude of the source region and on the presence and strength of the associated interplanetary

shock (Cane, Reames, and von Rosenvinge, 1988). In particular, particle time–intensity profiles, peak intensities, and power-law spectral indices have been found to be dependent on the longitude of the solar flare or CME causing the particle increase (Van Hollebeke, Ma Sung, and McDonald, 1975; Cane, Reames, and von Rosenvinge, 1988; Reames, Barbier, and Ng, 1996; Lario *et al.*, 2013). Longitude dependences are most significant in eastern events, while in the region magnetically well connected to the observer, roughly extending from 10W to 90W, variations in the parameters are much weaker. The longitude effects can also be studied as a function of the angular distance of the source region from the footpoint of the magnetic field line connecting to the observer. Strongly disturbed interplanetary conditions and wide-spread coronal shocks can, however, dissolve a simple dependence on the connection angle. In their study of wide-spread SEP events, Paassilta *et al.* (2018) concluded that there is no simple relation between the connection angle and the rise time or release delay of protons.

Our events cover the longitude range from 23E to 90W and a number of events beyond the west limb of the Sun, but with a large majority of events in the western solar hemisphere. Category 2 events cover the whole longitude range of 23E to > 90W, while Category 1 events mainly concentrate in the well-connected region. A possible dependence of the proton intensity rise rate on the connection angle was visible in our data, but in particular for Category 2 events covering a wide range of connection angles from $+19°$ to $-76°$, the dependence was only very weak ($r = 0.19 \pm 0.09$). Performing multiple linear regression by using $t_{o,p} - t_{\text{III}}$ and the connection angle as independent variables showed that the time difference $t_{o,p} - t_{\text{III}}$ was clearly more significant in explaining the overall behavior and correlated well with the rise rate as shown in Figure 8a. Figure 8a indicates that the average intensity rise rate of Category 1 events is higher than that of Category 2. It is noteworthy that although the average rise times were also significantly different between Category 1 and 2 events, the maximum intensities were not (see Table 1).

The onset times of protons at different energies observed at 1 AU, and thus the derived release times of protons, can depend on the connection angle (*e.g.* Rouillard *et al.*, 2012). In Figure 6a we plotted the difference between proton release time and decametric type III onset time as a function of the connection angle for the events in Category 1 and Category 2. Taken all events together, there is only a weak trend of increasing time difference $t_{o,p} - t_{\text{III}}$ when the connection angle is growing in the negative direction. In particular, there is a large scatter of the Category 2 events both in the time difference and in the connection angle with no correlation ($r = -0.002 \pm 0.091$) between these quantities. Thus, the time differences between the proton release and the type III onsets in Category 2 events are not explained by the connection angle. However, most of the Category 2 events have negative connection angles, while Category 1 events originate mainly from a restricted range of positive connection angles and also have less variation in the time difference.

To verify that the significant differences in the average values of several parameters shown in Table 1 is not explained by the connection angle, we investigated the properties of Category 1 and 2 events originating from the same connection angle region. Twelve events in both categories originated from the connection angle range $-30°$ to $+30°$. We performed the same tests for the average values of various characteristics of these selected events as for the entire Categories 1 and 2. We found that the significant differences (at $\geq 97\%$ confidence level) in the average values of Category 1 and Category 2 events were retained, except for the time differences involving the electron release time and the CME angular width and, due to the event selection criterion, the connection angle and longitude. In particular, the average values of the intensity rise rate, rise time, proton release height, and the difference between proton release time and type III onset time remained different at $> 99\%$ confidence

level. These results show that the differences in the characteristics of Category 1 and Category 2 events cannot be explained by a dependence on connection angle or on solar source longitude.

7.3. Proton Release Heights

We investigated the release heights of protons in Category 1 and Category 2 events derived from the CME leading front height–time data and from the shock height at the time of the proton release based on the hybrid atmospheric density model. The release heights given by the two methods agreed fairly well (Figure 7b), although there are also deviations between the methods possibly due to errors caused by extrapolating the height–time data below the coronagraph field of view, and reflecting the uncertainties in the location of the shock with respect to the CME structure. As well, difficulties in identifying type II lanes in some cases and possible incorrect associations of shocks with CMEs can lead to uncertainties. Noteworthy is that the model-based release heights of Category 1 and 2 events are clearly separate, while those given by the CME leading front height are overlapping. Both Figure 7a and Figure 7b show, however, that in Category 1 events protons are released low in the corona (1.1 to 2.6 $R_\odot$ based on shock height), whereas protons in Category 2 events are released in a wide range of heights from 2.8 to 9.5 $R_\odot$. In Category 1 events the acceleration mechanism can be a CME-driven shock low in the corona, but acceleration below the CME leading front, in solar flares or in processes related to CME initiation (Klein and Posner, 2005) cannot be excluded. There was no significant difference between the average release heights of those Category 1 events, which were associated with only m type II emission (11/18) compared to those associated with both m and DH type II. Missing DH type II emission implies that the CME is not strong enough to drive a shock high in the solar corona. In all but one Category 2 events in which only DH type II emission was observed, the release heights derived from the shock heights were above 4.0 $R_\odot$, and the time delays from the type III onsets to the proton release times were 15 minutes or more. The overall release height distribution of Figure 7a corresponds to the results of Kouloumvakos *et al.* (2015) using CME height–time data (their Figure 10). The distribution is also in agreement with other previous studies (*e.g.* Cliver, Kahler, and Reames, 2004; Reames, 2009; Gopalswamy *et al.*, 2012).

We used the observed type II starting frequencies and the hybrid atmospheric density model to derive the shock formation heights. The average heights for Category 1 and Category 2 events were 1.3 and 2.0 $R_\odot$. The average height of Category 1 events is in fairly good agreement with the average shock formation heights found by Gopalswamy *et al.* (2013) for 32 CMEs associated with metric type II bursts. On the other hand, the shock formation heights of Category 1 and 2 events are slightly lower than those reported by Prakash *et al.* (2017) for metric type II bursts (1.58 $R_\odot$) and for DH type II bursts (3.54 $R_\odot$) associated with SEP events. Prakash *et al.* (2017) determined the shock formation heights by back extrapolation of the CME heights assuming a constant CME speed.

Figure 8a showed a clear dependence of the proton intensity rise rate on the difference between the proton release time and type III onset time. The intensity rise rate is also strongly dependent ($r = -0.78 \pm 0.02$) on the release height as shown in Figure 8b. Generally, the rise rates of the Category 1 events are clearly higher than those of the Category 2 events. This can be due to a more impulsive acceleration of the particles in Category 1 events or slower acceleration and release process of the particles in Category 2 events.

7.4. Time-of-Maximum Energy Spectra

We determined the time-of-maximum energy spectra of protons in Category 1 and Category 2 events assuming a single-power-law form. In Figure 9 we presented the spectral

indices as a function of the proton release heights obtained from the shock height at the time of proton release given by the type II frequency and the hybrid density model. There is a quite significant overlap in the indices in Category 1 and Category 2. In Category 1 events the spectral index was in the range -1.70 to -3.43 and in Category 2 events in the range -1.85 to -4.62. The overlap mainly occurs in the spectral index range $\gamma > -3$. In Category 1, 75% of the events have a spectral index above this value, while 52% of Category 2 events have $\gamma < -3$. Therefore, the average values of the spectral index in Category 1 and 2 events are significantly different (Table 1) in spite of the overlap. As for several other parameters (see Section 7.2), there was no significant correlation between the spectral index and the longitude or connection angle. Those Category 2 events with spectral indices beyond the range of Category 1 indices were all western events, three of them from behind the west limb. Most of these events, however, had negative connection angles.

Traditionally solar energetic particle events have been divided into two classes of impulsive and gradual events (Cane, McGuire, and von Rosenvinge, 1986). Cane, Richardson, and von Rosenvinge (2010) and more recently Kim *et al.* (2014, 2015), Gopalswamy *et al.* (2015, 2016b, 2017), Miteva (2018) have presented divisions of SEP events in types or groups deviating from this traditional classification. Our Category 1 events are "impulsive" in the sense that they have high intensity rise rates, short rise times, the protons are released low in the corona, the events originate from magnetically well-connected regions, and are associated with short-duration X-ray flares. However, there is no significant difference in the maximum intensity of Category 1 and Category 2 events, and Category 1 events on the average have harder energy spectra than Category 2 events.

Recently Gopalswamy *et al.* (2017) (see also Gopalswamy *et al.*, 2015, 2016b) suggested that SEP events can be organized by the kinematic properties of CMEs. Gopalswamy *et al.* (2016b) found a hierarchical relationship between CME initial acceleration and the fluence spectrum power-law index. SEP events were divided into three groups: events related to eruptive filaments had the softest spectrum, lowest CME initial acceleration, and largest shock formation height, while ground level enhancement (GLE) events had the hardest spectrum, largest initial acceleration, and lowest shock formation height. The third group, regular SEP events, had intermediate spectral indices and acceleration (Gopalswamy *et al.*, 2016b). For GLE events Gopalswamy *et al.* (2017) give the average shock formation height of 1.51 $R_\odot$, which is slightly higher than the average in our Category 1 events (1.3 $R_\odot$). This can be considered even surprising, because our Category 1 events include only three GLEs. The average slope of the time-of-maximum energy spectra for Category 1 events was -2.55 ± 0.13 (Table 1), which is comparable with the average fluence spectral index 2.68 of the GLE events of Gopalswamy *et al.* (2016b). The average CME initial acceleration in Category 1 events was (1.7 ± 0.3) km s^{-2}, which corresponds to the average initial acceleration of the regular SEP events of Gopalswamy *et al.* (2016b), whereas the initial acceleration of Category 2 events was closer to the filament eruption events. We did not find statistically significant difference between the average CME initial accelerations in Category 1 and 2 events. Taken all our events together, there was a weak correlation ($r = 0.24 \pm 0.13$) between the spectral index and the CME initial acceleration. For Category 1 events alone the correlation was stronger ($r = 0.39 \pm 0.18$), while there was no correlation ($r = 0.19 \pm 0.13$) for Category 2 events. The shock formation heights and the differences between the proton release times and decametric type III onset times showed comparable weak or no dependences on the CME initial acceleration.

7.5. Electron Events Temporally Related to Proton Events

When analyzing the release times of electrons in events temporally related to the proton events, we found two main groups: in one group of events protons were released within tim-

ing uncertainties simultaneously (release time differences in the range $[-6, +7]$ minutes) with electrons, while in the other group proton release was delayed with respect to the electrons on average by 18 minutes (range $[+9, +42]$ minutes). In only one event electrons were released later than protons. The portions of simultaneous and delayed proton events in the total 36 electron events were 53% and 44%. The portion of simultaneous events is slightly less than reported by Xie *et al.* (2016), who found that in $\sim 70\%$ of their high-energy proton and electron events the particles were released simultaneously within 8 minutes, while in the rest 30% proton release was delayed by $\sim 8 - 31$ minutes. On the other hand, Kouloumvakos *et al.* (2015) found that in about half of their 34 events protons and electrons were released simultaneously, but in the other half electrons were released later than protons, on average by about 7 minutes.

The time differences of electron and proton release times with respect to type III onsets are well organized (Figure 5a), but there is more scatter in the delayed proton events. As well, we found in our data set a clear dependence of the difference between the proton and electron release times on the difference between the proton release times and the type III onsets (Figure 5b). This is contrary to the finding of Kouloumvakos *et al.* (2015) (their Figure 8), who defined several groups of events, but found no clear dependences in the time differences.

In Figure 6b we presented the dependence of the difference between the electron release time and type III onset on the connection angle for the simultaneous and delayed events. For the simultaneous events, which concentrate in a relatively limited range of connection angles, the time difference is slightly increasing with increasing negative connection angle. For the delayed proton events such dependence is not evident. Figure 6b can be compared with the results of Xie *et al.* (2016) (their Figure 8), who found only a poor correlation between the time difference and the connection angle in their electron events. About half of our delayed proton events had connection angles in the same range as the simultaneous events. At least in these events the difficulty to access open magnetic field lines leading to the observer at 1 AU cannot explain the delay.

When considering all 58 proton events and all 36 temporally related electron events, we found that the average path lengths of protons and electrons were equal within the error limits: (1.50 ± 0.05) AU for protons and (1.58 ± 0.08) AU for electrons. Kouloumvakos *et al.* (2015) obtained for their 34 proton and electron events considerably longer average path lengths for protons compared to electrons. We used in our analysis a more limited energy range for protons, which we believe to give the most reliable results. Assuming the solar release time of electrons to be equal to the onset time of metric type II or DH type III radio burst, Tan *et al.* (2013) found the path length of low-energy electrons to be consistent with the ion path length, but increasing with energy, which they attributed to pitch angle scattering of high-energy electrons.

Krucker and Lin (2000) have reported of two classes of electron and proton events with different proton path lengths in the two classes. In one class, protons and electrons had the same path lengths in the range $1.1 - 1.3$ AU, but proton injection was significantly delayed with respect to electrons. In the second class protons and electrons were released simultaneously within uncertainties, but protons had apparent path lengths around 2 AU, whereas electrons had the same path lengths as in the first class. The longer path lengths of protons were explained by a later release of successively lower-energy protons, although all protons were accelerated simultaneously high in the corona. We found the average path lengths of protons and electrons in the simultaneous proton and electron events to be equal: (1.51 ± 0.06) AU for protons and (1.51 ± 0.11) AU for electrons. In the events where proton release time was later than electrons, the average electron path length was slightly longer, (1.65 ± 0.13) AU, but within uncertainties the same as in the simultaneous events. In these events the average

path length of protons was (1.25 ± 0.06) AU, which is significantly shorter that the path lengths in the simultaneous events. It is improbable that protons would travel a shorter distance than electrons in the same events. The cause of the apparently shorter path length could be an energy and time-dependent acceleration or release of protons. If protons at successively higher energies are systematically accelerated or released later than at lower energies, then the onsets at successively higher energies would also be observed later at 1 AU leading to shorter path lengths given by VDA. Compared to our proton energy range, Krucker and Lin (2000) investigated protons at significantly lower energies between $\sim 0.03-6$ MeV. Based on a preliminary analysis of one event Krucker and Lin (2000) suggested that the release time of high-energy (~ 70 MeV) protons might be simultaneous with near-relativistic electrons. Xie *et al.* (2016), however, found several events with large delays of ~ 90 MeV protons with respect to 0.5 MeV electrons.

Timing analysis showed that the time difference between the proton release time and the type III onset in the delayed proton events was generally much larger than in the simultaneous events, and in 75% of the delayed proton events protons were released after the end of type III burst. This suggests a late acceleration or release of protons in the delayed events. It should be recalled, however, that the simultaneous and delayed events did not generally comply with the Category 1 and Category 2 division of the proton events, although only two of the delayed proton events belonged to Category 1. A simple scenario of delayed proton acceleration by CME-driven shocks at higher altitudes and thus at later times is not a fully satisfactory explanation, and the exact cause for the delay remains unsolved.

While the 36 temporally related proton and electron events consisted of 19 simultaneous proton and electron events and of 16 delayed proton events, there was only one delayed electron event. In this event, electrons were released 10 minutes after protons, but with only 4 minute margin when the release time uncertainties were taken into account. This was also the only event for which VDA gave a proton release time before the decametric type III onset with a time difference of -3 minutes. Electrons were released during the type III emission. The uncertainty of the proton release time was ± 2 minutes. Thus, only one minute additional uncertainty in the proton release time would have made this event simultaneous with the type III onset, and an additional total uncertainty of 4 minutes in the proton and electron release times would have made this event also a simultaneous proton and electron event. There was, however, one exceptional property in this event: it was the only Category 1 proton event with a temporally related electron event, which was associated with both m and DH type II emission. Taking into account the uncertainty in the electron release time, the margin between the electron release and the DH type II onset was 4 minutes. In addition to the delayed electron event, there were eight proton events with electron event counterparts in Category 1, but these six simultaneous and two delayed proton events were associated with only m type II emission. The delayed electron event had a connection angle of $-2°$. The proton release height given by the CME height–time data was 4.4 $R_\odot$ (the only Category 1 event in bin 4 of Figure 7), whereas the release height based on the shock height was 1.8 $R_\odot$. As for the delayed proton events, the nature of this delayed electron event remains unclear: was it erroneously classified due to inadequately estimated uncertainties in the release times, or were the electrons genuinely accelerated or released later than protons *e.g.* by a CME-driven shock high in the corona close to the time of the DH type II onset.

8. Conclusions

We have investigated the properties of solar energetic particle events and their associations and the release times of the particles relative to type II, III, and IV radio bursts, as these are

related to propagating shock waves, electron beams, and trapped particles, respectively. Almost all proton events (56/58) were associated with type II emission and all were associated with type III. In one event protons were released before the decametric type III onset, in 19 events after the type III burst had ended, while in most events (64%) the release occurred during the type III emission. Metric type IV emission was observed in 55% of the events, whereas DH type IV was not associated with any of the events.

We found that proton events associated with only metric type II radio emission or with m-DH type II emission with protons released before the DH type II onset (Category 1 events) exhibit different characteristics compared to proton events associated with only DH type II emission or with m-DH emission, but with protons released at or after the DH type II onset (Category 2 events). We conclude that protons in the Category 2 events are accelerated high in the corona, presumably in CME-driven shocks strong enough to survive up to the heights where DH type II emission is produced. If protons in the Category 1 events are also accelerated by CME-driven shocks, the acceleration occurs low in the corona. Uncertainties in the proton release times and CME heights do not exclude acceleration below the heights of the CME leading front, in flare or CME initiation related processes.

When investigating the relative release times of protons and electrons, we found that in most events (53%) protons and electrons were released and presumably also accelerated simultaneously within ± 7 minutes. In the rest of the events proton release was delayed with respect to electrons, with the exception of one event in which electrons were released later than protons. The simultaneous and delayed events did not unambiguously fall in the two categories of proton events based on the type II associations, although only two delayed proton events and the single delayed electron event belonged to Category 1. Our investigation was not conclusive for the cause of the delays.

Appendix

Table 2   Event list with proton VDA results and onset times of associated solar radio emissions, soft X-ray flares, and CMEs.

No.	Date[a] dd.mm.yy	Proton VDA[b]		Radio onset[c]				SXR[d]		$\Delta\phi$ °	CME[e] 1st obs. UT
		$t_{\circ,p}$[f] UT	s_p AU	t_{III} UT	$t_{\mathrm{m\text{-}II}}$ UT	$t_{\mathrm{DH\text{-}II}}$ UT	$t_{\mathrm{m\text{-}IV}}$ UT	Onset UT	Location		
1	04.11.97	$06{:}16 \pm 02^2$	1.48 ± 0.05	05:56	05:58	06:00	06:06	05:52	14S33W	−46	06:10
2	09.05.98	$03{:}52 \pm 04^2$	2.08 ± 0.12	03:22*	03:26*	03:35*	03:23*	03:04	100W*	⋯	03:35

Table 2 (*Continued*)

No.	Date[a] dd.mm.yy	Proton VDA[b] $t_{\circ,p}$[f] UT	s_p AU	Radio onset[c] t_{III} UT	$t_{m\text{-}II}$ UT	$t_{DH\text{-}II}$ UT	$t_{m\text{-}IV}$ UT	SXR[d] Onset UT	Location	$\Delta\phi$ °	CME[e] 1st obs. UT
3	22.11.98	$06:52\pm05^1$	1.34 ± 0.12	06:41	06:38	No	No	06:30	27S82W	21	dg
4	09.05.99	$18:27\pm04$	0.98 ± 0.10	17:59*	No	No	No	17:53	95W*	⋯	18:27
5	01.06.99	$19:22\pm03^2$	1.68 ± 0.08	18:44*	No	18:50*	No	18:53	120W*	⋯	19:37
6	11.06.99	$00:48\pm05^1$	1.36 ± 0.13	00:41*	00:39*	No	00:51*	01:05	120W*	⋯	01:26
7	17.02.00	$20:57\pm03^2$	1.31 ± 0.08	20:29	20:25	20:42	No	20:17	29S07E	−70	21:30
8	18.02.00	$09:37\pm03^3$	1.39 ± 0.08	09:20	09:13	09:44	No	09:21	120W*	⋯	09:54
9	02.03.00	$08:49\pm02^1$	1.30 ± 0.05	08:25	08:27	No	08:23	08:20	14S52W	−5	08:54
10	03.03.00	$02:22\pm04^1$	1.65 ± 0.10	02:12	02:12	No	02:18	02:08	15S60W	1	02:30
11	04.04.00	$15:43\pm06^2$	0.94 ± 0.17	15:17	15:25	15:45	15:15	15:12	16N66W	0	16:32
12	10.06.00	$17:10\pm02^3$	1.09 ± 0.05	16:56	16:55	17:15	No	16:40	22N40W	−10	17:08
13	18.06.00	$01:57\pm06^1$	1.80 ± 0.13	01:57	01:57	No	No	01:52	23N85W	23	02:10
14	22.07.00	$11:27\pm02^1$	2.23 ± 0.03	11:30	11:25	11:45	11:18	11:17	14N56W	−2	11:54
15	12.09.00	$12:45\pm03^2$	1.25 ± 0.06	11:46	11:33	12:00	Yes?[g]	11:31	17S09W	−58	11:54
16	28.01.01	$16:06\pm09^2$	2.51 ± 0.26	15:46	No	15:45	No	15:40	04S59W	−16	15:54
17	29.03.01	$10:49\pm05^2$	1.06 ± 0.16	09:59	10:03	10:12	09:58	09:57	20N19W	−29	10:26
18	02.04.01	$12:12\pm09^2$	1.62 ± 0.20	11:00	11:10	11:30	11:06	10:58	16N62W	19	11:26
19	15.04.01	$13:40\pm04^1$	1.50 ± 0.14	13:39	13:47	14:05	13:52	13:19	20S85W	33	14:06
20	18.04.01	$02:16\pm07^1$	1.97 ± 0.19	02:16*	02:17*	02:55*	02:20*	02:11	120W*	⋯	02:30
21	07.05.01	$12:09\pm03^2$	2.43 ± 0.09	NA	No?	12:00*	No	11:36	120W*	⋯	12:06
22	20.05.01	$06:37\pm06^1$	1.02 ± 0.16	06:08*	06:04*	No	No	06:00	17S91W*	⋯	06:26
23	04.06.01	$16:43\pm07^1$	1.35 ± 0.15	16:22	16:14	No	No	16:11	24N59W	1	16:30
24	15.06.01	$15:57\pm05^3$	1.12 ± 0.12	15:34*	15:33*	16:05*	No	⋯	120W*	⋯	15:56
25	19.06.01	$03:57\pm07^1$	1.27 ± 0.23	03:38*	03:35*	No	No	⋯	⋯	⋯	03:54
26	24.09.01	$10:55\pm04^2$	1.39 ± 0.12	10:18	No	10:45	09:59	09:32	16S23E	−76	10:30
27	19.10.01	$01:14\pm08^2$	2.50 ± 0.20	01:03	00:59	01:15	00:58	00:47	16N18W	−21	01:27
28	22.10.01	$15:26\pm03^2$	1.27 ± 0.06	15:02	14:53	15:15	14:45	14:27	21S18E	−36	15:06
29	22.11.01	$20:21\pm05^1$	1.98 ± 0.12	20:24	20:22	20:50	No	20:18	25S67W	11	20:30
30	26.12.01	$05:23\pm10^2$	1.47 ± 0.29	05:13	04:59	05:20	05:01	04:32	08N54W	−10	05:30
31	27.01.02	$13:07\pm06^2$	1.92 ± 0.15	NA	No?	12:49*	No	⋯	120W*	⋯	12:30
32	20.02.02	$06:03\pm03^1$	1.08 ± 0.08	05:55	06:15	No	06:21	05:52	12N72W	8	06:30
33	07.07.02	$11:51\pm05^2$	1.30 ± 0.09	11:17*	No	11:35*	No	11:15	95W*	⋯	11:30
34	18.08.02	$21:34\pm10^1$	1.84 ± 0.28	21:15	21:24	No	21:36	21:12	12S19W	−25	21:54
35	20.08.02	$08:27\pm02$	1.21 ± 0.05	08:24	No	No	No	08:22	10S38W	−15	08:54
36	22.08.02	$02:13\pm06^1$	1.09 ± 0.17	01:50	01:55	No	02:10	01:47	07S62W	1	02:06
37	24.08.02	$00:58\pm06^1$	2.02 ± 0.24	00:51	01:01	01:45	01:15	00:49	02S81W	14	01:27
38	09.11.02	$14:08\pm16^2$	1.51 ± 0.46	13:08	13:17	13:20	13:07	13:08	12S29W	−38	13:31
39	19.12.02	$22:03\pm07^2$	1.06 ± 0.16	21:41	21:39	21:45	21:39	21:34	15N09W	−39	22:06
40	31.05.03	$02:48\pm07^3$	1.04 ± 0.20	02:21	02:20	03:00	02:18	02:13	07S65W	30	02:30
41	11.04.04	$04:42\pm02^2$	1.28 ± 0.05	03:58	No	04:20	No	03:54	16S46W	−13	04:30
42	01.11.04	$05:57\pm05^2$	1.41 ± 0.14	05:42*	No?	05:55*	No	⋯	120W*	⋯	06:06
43	16.06.05	$20:21\pm03^3$	1.28 ± 0.07	20:12	20:10	20:25	20:17	20:01	08N90W	50	dg

Table 2 (*Continued*)

No.	Date[a] dd.mm.yy	Proton VDA[b] $t_{\circ,p}$[f] UT	s_p AU	Radio onset[c] t_{III} UT	$t_{\text{m-II}}$ UT	$t_{\text{DH-II}}$ UT	$t_{\text{m-IV}}$ UT	SXR[d] Onset UT	Location	$\Delta\phi$ °	CME[e] 1st obs. UT
44	14.08.10	$10:19 \pm 03^2$	1.12 ± 0.08	09:56	09:50	10:00	09:37	09:38	17N52W	−12	10:12
45	28.01.11	$01:33 \pm 10^2$	1.34 ± 0.33	01:04	01:02	01:15	No	00:44	16N88W	5	01:26
46	07.03.11	$20:33 \pm 07^2$	1.81 ± 0.18	19:52	19:54	20:00	20:00	19:43	30N48W	−21	20:00
47	21.03.11	$02:47 \pm 05^2$	1.90 ± 0.16	02:21*	02:20*	02:30*	02:20*	$\cdots$	138W*	$\cdots$	02:24
48	04.08.11	$04:12 \pm 04^2$	1.91 ± 0.12	03:52	03:54	04:15	03:50	03:41	19N36W	−39	04:12
49	08.08.11	$18:12 \pm 04^2$	1.27 ± 0.13	18:04	18:07	18:10	18:05	18:00	16N61W	17	18:12
50	09.08.11	$08:07 \pm 04^1$	0.96 ± 0.11	08:02	08:01	08:20	08:01	07:48	17N69W	25	08:12
51	06.09.11	$02:10 \pm 05^2$	1.10 ± 0.13	01:49	01:45	02:00	02:27	01:35	14N07W	−58	02:24
52	13.03.12	$17:28 \pm 05^3$	1.49 ± 0.16	17:21	17:15	17:35	17:30	17:12	17N66W	21	17:36
53	17.07.12	$14:50 \pm 05^2$	1.43 ± 0.20	14:02	No	14:40	14:00	12:03	28S65W	12	13:48
54	08.09.12	$11:02 \pm 06^2$	1.49 ± 0.19	NA	No?	09:45*	No	$\cdots$	145W*	$\cdots$	10:00
55	20.02.14	$07:51 \pm 03^1$	1.17 ± 0.08	07:48	07:45	08:05	No	07:26	15S73W	33	08:00
56	25.08.14	$16:05 \pm 19^2$	1.92 ± 0.50	14:55	15:12	15:20	Yes?	14:46	05N36W	−51	15:36
57	22.09.14	$06:40 \pm 06^2$	1.81 ± 0.14	06:21*	No	06:13*	No	$\cdots$	$\cdots$	$\cdots$	06:12
58	01.07.15	$14:52 \pm 02^3$	1.67 ± 0.05	14:44*	14:38*	16:08*	No	$\cdots$	$\cdots$	$\cdots$	14:36

[a]Date of the SEP event onset.

[b]$t_{\circ,p}$ and s_p refer to the proton release time and path length, respectively.

[c]t_{III}, $t_{\text{m-II}}$, $t_{\text{DH-II}}$, and $t_{\text{m-IV}}$ refer to the onset times of decametric type III, metric, decametric–hectometric type II, and metric type IV radio bursts, respectively. "No" means that the radio burst was not observed in the data, "NA" means that observations were not available, and "?" refers to uncertainty. Onset times marked with "*" are the first appearances for backside events.

[d]Ellipsis means that the data of soft X-ray flare are not known. The locations marked with "*" are from Cane, Richardson, and von Rosenvinge (2010) and Richardson *et al.* (2014) for backside events in SCs 23 and 24, respectively. These events were not included in the analysis, where flare location was required.

[e]Time of first appearance of the CME in LASCO/C2.

[f]"1", "2" and "3" refer to proton events in Category 1, Category 2, and the unclear events, respectively.

[g]A type IV burst was listed in Klein *et al.* (2005), based on observations by the *Nançay Radioheliograph* (NRH).

Table 3 VDA results for the 36 solar electron events associated with the proton events.

No.[a]	Date dd.mm.yy	Electron VDA[b] $t_{\circ,e}$ UT	s_e AU	S/D[c]	No.[a]	Date dd.mm.yy	Electron VDA[b] $t_{\circ,e}$ UT	s_e AU	S/D[c]
1	04.11.97	$06:22 \pm 06$	1.85 ± 0.40	S	35	20.08.02	$08:29 \pm 02$	1.59 ± 0.10	S
3	22.11.98	$06:58 \pm 02$	1.39 ± 0.12	S	36	22.08.02	$02:14 \pm 04$	1.14 ± 0.30	S
4	09.05.99	$18:13 \pm 03$	1.14 ± 0.12	D	38	09.11.02	$13:41 \pm 05$	1.58 ± 0.26	D
5	01.06.99	$19:19 \pm 04$	1.49 ± 0.27	S	39	19.12.02	$21:58 \pm 02$	0.98 ± 0.07	S
6	11.06.99	$00:51 \pm 02$	1.15 ± 0.08	S	40	31.05.03	$02:23 \pm 05$	1.86 ± 0.28	D
7	17.02.00	$20:46 \pm 05$	2.95 ± 0.31	D	41	11.04.04	$04:20 \pm 04$	1.39 ± 0.22	D
9	02.03.00	$08:36 \pm 02$	1.25 ± 0.07	D	42	01.11.04	$05:52 \pm 04$	1.42 ± 0.19	S
10	03.03.00	$02:24 \pm 02$	1.07 ± 0.11	S	43	16.06.05	$20:26 \pm 04$	1.05 ± 0.16	S

Table 3 (*Continued*)

No.[a]	Date dd.mm.yy	Electron VDA[b]			No.[a]	Date dd.mm.yy	Electron VDA[b]		
		$t_{\circ,e}$ UT	s_e AU	S/D[c]			$t_{\circ,e}$ UT	s_e AU	S/D[c]
13	18.06.00	$02{:}03 \pm 02$	1.54 ± 0.07	S	44	14.08.10	$10{:}10 \pm 02$	1.04 ± 0.07	D
14	22.07.00	$11{:}37 \pm 04$	1.63 ± 0.18	De	45	28.01.11	$01{:}16 \pm 06$	1.70 ± 0.34	D
15	12.09.00	$12{:}34 \pm 03$	1.13 ± 0.14	D	46	07.03.11	$20{:}34 \pm 08$	1.45 ± 0.55	S
17	29.03.01	$10{:}07 \pm 05$	1.86 ± 0.25	D	47	21.03.11	$02{:}45 \pm 09$	2.26 ± 0.52	S
22	20.05.01	$06{:}18 \pm 03$	1.67 ± 0.19	D	48	04.08.11	$04{:}14 \pm 04$	1.71 ± 0.16	S
23	04.06.01	$16{:}38 \pm 03$	0.98 ± 0.12	S	51	06.09.11	$01{:}54 \pm 02$	1.53 ± 0.09	D
24	15.06.01	$15{:}41 \pm 03$	1.56 ± 0.15	D	52	13.03.12	$17{:}30 \pm 05$	2.59 ± 0.25	S
26	24.09.01	$10{:}46 \pm 03$	1.81 ± 0.19	D	56	25.08.14	$15{:}27 \pm 08$	2.53 ± 0.50	D
30	26.12.01	$05{:}28 \pm 02$	0.97 ± 0.15	S	57	22.09.14	$06{:}33 \pm 06$	2.48 ± 0.28	S
33	07.07.02	$11{:}42 \pm 02$	1.45 ± 0.06	D	58	01.07.15	$14{:}55 \pm 02$	1.55 ± 0.11	S

[a]The numbering of the events is the same as used in Table 2.

[b]$t_{\circ,e}$ and s_e refer to the electron release time and path length, respectively.

[c]S, D, and De refer to simultaneous proton and electron events, delayed proton events, and the delayed electron event, respectively.

References

Benz, A.O.: 1980, Electron trapping in the solar magnetic field and emission of decimetric continuum radio bursts. *Astrophys. J.* **240**, 892. DOI. ADS.

Bougeret, J.-L., Kaiser, M.L., Kellogg, P.J., Manning, R., Goetz, K., Monson, S.J., Monge, N., Friel, L., Meetre, C.A., Perche, C., Sitruk, L., Hoang, S.: 1995, Waves: The radio and plasma wave investigation on the Wind Spacecraft. *Space Sci. Rev.* **71**, 231. DOI. ADS.

Brueckner, G.E., Howard, R.A., Koomen, M.J., Korendyke, C.M., Michels, D.J., Moses, J.D., Socker, D.G., Dere, K.P., Lamy, P.L., Llebaria, A., Bout, M.V., Schwenn, R., Simnett, G.M., Bedford, D.K., Eyles, C.J.: 1995, The Large Angle Spectroscopic Coronagraph (LASCO). *Solar Phys.* **162**, 357. DOI. ADS.

Cairns, I.H., Knock, S.A., Robinson, P.A., Kuncic, Z.: 2003, Type II solar radio bursts: Theory and space weather implications. *Space Sci. Rev.* **107**, 27. DOI. ADS.

Cane, H.V., Erickson, W.C., Prestage, N.P.: 2002, Solar flares, type III radio bursts, coronal mass ejections, and energetic particles. *J. Geophys. Res.* **107**, 1315. DOI. ADS.

Cane, H.V., McGuire, R.E., von Rosenvinge, T.T.: 1986, Two classes of solar energetic particle events associated with impulsive and long-duration soft X-ray flares. *Astrophys. J.* **301**, 448. DOI. ADS.

Cane, H.V., Reames, D.V., von Rosenvinge, T.T.: 1988, The role of interplanetary shocks in the longitude distribution of solar energetic particles. *J. Geophys. Res.* **93**, 9555. DOI. ADS.

Cane, H.V., Richardson, I.G., von Rosenvinge, T.T.: 2010, A study of solar energetic particle events of 1997 – 2006: Their composition and associations. *J. Geophys. Res.* **115**, A08101. DOI. ADS.

Cantrell, C.A.: 2008, Technical note: Review of methods for linear least-squares fitting of data and application to atmospheric chemistry problems. *Atmos. Chem. Phys. Discuss.* **8**, 6409. ADS.

Cliver, E.W., Kahler, S.W., Reames, D.V.: 2004, Coronal shocks and solar energetic proton events. *Astrophys. J.* **605**, 902. DOI. ADS.

Cliver, E.W., Ling, A.G.: 2009, Low-frequency type III bursts and solar energetic particle events. *Astrophys. J.* **690**, 598. DOI. ADS.

Gopalswamy, N.: 2003, Solar and geospace connections of energetic particle events. *Geophys. Res. Lett.* **30**, 8013. DOI. ADS.

Gopalswamy, N., Aguilar-Rodriguez, E., Yashiro, S., Nunes, S., Kaiser, M.L., Howard, R.A.: 2005, Type II radio bursts and energetic solar eruptions. *J. Geophys. Res.* **110**, A12S07. DOI. ADS.

Gopalswamy, N., Yashiro, S., Michalek, G., Xie, H., Mäkelä, P., Vourlidas, A., Howard, R.A.: 2010, A catalog of halo coronal mass ejections from SOHO. *Sun Geosph.* **5**, 7. ADS.

Gopalswamy, N., Xie, H., Yashiro, S., Akiyama, S., Mäkelä, P., Usoskin, I.G.: 2012, Properties of ground level enhancement events and the associated solar eruptions during Solar Cycle 23. *Space Sci. Rev.* **171**, 23. DOI. ADS.

Gopalswamy, N., Xie, H., Mäkelä, P., Yashiro, S., Akiyama, S., Uddin, W., Srivastava, A.K., Joshi, N.C., Chandra, R., Manoharan, P.K.: 2013, Height of shock formation in the solar corona inferred from observations of type II radio bursts and coronal mass ejections. *Adv. Space Res.* **51**(11), 1981. DOI. ADS.

Gopalswamy, N., Mäkelä, P., Akiyama, S., Yashiro, S., Xie, H., Thakur, N., Kahler, S.W.: 2015, Large solar energetic particle events associated with filament eruptions outside of active regions. *Astrophys. J.* **806**, 8. DOI. ADS.

Gopalswamy, N., Akiyama, S., Mäkelä, P., Yashiro, S., Cairns, I.H.: 2016a, On the directivity of low-frequency type IV radio bursts. In: *URSI Asia-Pacific Radio Science Conference in Seoul*, *August 21 – 25, 2016*. ADS.

Gopalswamy, N., Yashiro, S., Thakur, N., Mäkelä, P., Xie, H., Akiyama, S.: 2016b, The 2012 July 23 backside eruption: An extreme energetic particle event? *Astrophys. J.* **833**, 216. DOI. ADS.

Gopalswamy, N., Mäkelä, P., Yashiro, S., Thakur, N., Akiyama, S., Xie, H.: 2017, A hierarchical relationship between the fluence spectra and CME kinematics in large solar energetic particle events: A radio perspective. In: *Journal of Physics Conference Series*, *Journal of Physics Conference Series* **900**, 012009. DOI. ADS.

Hillaris, A., Bouratzis, C., Nindos, A.: 2016, Interplanetary type IV bursts. *Solar Phys.* **291**, 2049. DOI. ADS.

Huttunen-Heikinmaa, K., Valtonen, E., Laitinen, T.: 2005, Proton and helium release times in SEP events observed with SOHO/ERNE. *Astron. Astrophys.* **442**, 673. DOI. ADS.

Kahler, S., Ragot, B.R.: 2006, Near-relativistic electron c/v onset plots. *Astrophys. J.* **646**, 634. DOI. ADS.

Kim, R.-S., Cho, K.-S., Lee, J., Bong, S.-C., Park, Y.-D.: 2014, A refined classification of SPEs based on the multienergy channel observations. *J. Geophys. Res.* **119**, 9419. DOI. ADS.

Kim, R.-S., Cho, K.-S., Lee, J., Bong, S.-C., Joshi, A.D., Park, Y.-D.: 2015, Characteristics of four SPE groups with different origins and acceleration processes. *J. Geophys. Res.* **120**, 7083. DOI. ADS.

Klein, K.-L., Posner, A.: 2005, The onset of solar energetic particle events: Prompt release of deka-MeV protons and associated coronal activity. *Astron. Astrophys.* **438**, 1029. DOI. ADS.

Klein, K.-L., Krucker, S., Trottet, G., Hoang, S.: 2005, Coronal phenomena at the release of solar energetic electron events. *Astron. Astrophys.* **431**, 1047. DOI. ADS.

Klein, K.-L., Krucker, S., Lointier, G., Kerdraon, A.: 2008, Open magnetic flux tubes in the corona and the transport of solar energetic particles. *Astron. Astrophys.* **486**, 589. DOI. ADS.

Kouloumvakos, A., Nindos, A., Valtonen, E., Alissandrakis, C.E., Malandraki, O., Tsitsipis, P., Kontogeorgos, A., Moussas, X., Hillaris, A.: 2015, Properties of solar energetic particle events inferred from their associated radio emission. *Astron. Astrophys.* **580**, A80. DOI. ADS.

Krucker, S., Lin, R.P.: 2000, Two classes of solar proton events derived from onset time analysis. *Astrophys. J. Lett.* **542**, L61. DOI. ADS.

Laitinen, T., Huttunen-Heikinmaa, K., Valtonen, E., Dalla, S.: 2015, Correcting for interplanetary scattering in velocity dispersion analysis of solar energetic particles. *Astrophys. J.* **806**, 114. DOI. ADS.

Lario, D., Aran, A., Gómez-Herrero, R., Dresing, N., Heber, B., Ho, G.C., Decker, R.B., Roelof, E.C.: 2013, Longitudinal and radial dependence of solar energetic particle peak intensities: STEREO, ACE, SOHO, GOES, and MESSENGER observations. *Astrophys. J.* **767**, 41. DOI. ADS.

Leblanc, Y., Dulk, G.A., Bougeret, J.-L.: 1998, Tracing the electron density from the corona to 1 AU. *Solar Phys.* **183**, 165. DOI. ADS.

Lin, R.P.: 1985, Energetic solar electrons in the interplanetary medium. *Solar Phys.* **100**, 537. DOI. ADS.

Lin, R.P., Anderson, K.A., Ashford, S., Carlson, C., Curtis, D., Ergun, R., Larson, D., McFadden, J., McCarthy, M., Parks, G.K., Rème, H., Bosqued, J.M., Coutelier, J., Cotin, F., D'Uston, C., Wenzel, K.-P., Sanderson, T.R., Henrion, J., Ronnet, J.C., Paschmann, G.: 1995, A three-dimensional plasma and energetic particle investigation for the Wind Spacecraft. *Space Sci. Rev.* **71**, 125. DOI. ADS.

Lintunen, J., Vainio, R.: 2004, Solar energetic particle event onset as analyzed from simulated data. *Astron. Astrophys.* **420**, 343. DOI. ADS.

Markwardt, C.B.: 2009, Non-linear least-squares fitting in IDL with MPFIT. In: Bohlender, D.A., Durand, D., Dowler, P. (eds.) *Astronomical Data Analysis Software and Systems XVIII*, *Astronomical Society of the Pacific Conference Series* **411**, 251. ADS.

Miteva, R.: 2018, Solar radio bursts: Implications to the origin of *in situ* particles. *Sun Geosph.* **13**, 145. DOI. ADS.

Miteva, R., Klein, K.-L., Malandraki, O., Dorrian, G.: 2013, Solar energetic particle events in the 23rd solar cycle: Interplanetary magnetic field configuration and statistical relationship with flares and CMEs. *Solar Phys.* **282**, 579. DOI. ADS.

Nindos, A., Aurass, H., Klein, K.-L., Trottet, G.: 2008, Radio emission of flares and coronal mass ejections. Invited Review. *Solar Phys.* **253**, 3. DOI. ADS.

Paassilta, M., Raukunen, O., Vainio, R., Valtonen, E., Papaioannou, A., Siipola, R., Riihonen, E., Dierckxsens, M., Crosby, N., Malandraki, O., Heber, B., Klein, K.-L.: 2017, Catalogue of 55 – 80 MeV solar proton events extending through solar cycles 23 and 24. *J. Space Weather Space Clim.* **7**(27), A14. DOI. ADS.

Paassilta, M., Papaioannou, A., Dresing, N., Vainio, R., Valtonen, E., Heber, B.: 2018, Catalogue of > 55 MeV wide-longitude solar proton events observed by SOHO, ACE, and the STEREOs at ≈ 1 AU during 2009 – 2016. *Solar Phys.* **293**, 70. DOI. ADS.

Prakash, O., Feng, L., Michalek, G., Gan, W., Lu, L., Shanmugaraju, A., Umapathy, S.: 2017, Characteristics of events with metric-to-decahectometric type II radio bursts associated with CMEs and flares in relation to SEP events. *Astrophys. Space Sci.* **362**, 56. DOI. ADS.

Reames, D.V.: 1999, Particle acceleration at the Sun and in the heliosphere. *Space Sci. Rev.* **90**, 413. DOI. ADS.

Reames, D.V.: 2009, Solar release times of energetic particles in ground-level events. *Astrophys. J.* **693**, 812. DOI. ADS.

Reames, D.V., Barbier, L.M., Ng, C.K.: 1996, The spatial distribution of particles accelerated by coronal mass ejection–driven shocks. *Astrophys. J.* **466**, 473. DOI. ADS.

Richardson, I.G., von Rosenvinge, T.T., Cane, H.V., Christian, E.R., Cohen, C.M.S., Labrador, A.W., Leske, R.A., Mewaldt, R.A., Wiedenbeck, M.E., Stone, E.C.: 2014, > 25 MeV proton events observed by the high energy telescopes on the STEREO A and B spacecraft and/or at Earth during the first ∼ seven years of the STEREO mission. *Solar Phys.* **289**, 3059. DOI. ADS.

Rouillard, A.P., Sheeley, N.R., Tylka, A., Vourlidas, A., Ng, C.K., Rakowski, C., Cohen, C.M.S., Mewaldt, R.A., Mason, G.M., Reames, D., Savani, N.P., StCyr, O.C., Szabo, A.: 2012, The longitudinal properties of a solar energetic particle event investigated using modern solar imaging. *Astrophys. J.* **752**, 44. DOI. ADS.

Saito, K., Makita, M., Nishi, K., Hata, S.: 1970, A non-spherical axisymmetric model of the solar K corona of the minimum type. *Ann. Tokyo Astron. Obs.* **12**, 53. ADS.

Sáiz, A., Evenson, P., Ruffolo, D., Bieber, J.W.: 2005, On the estimation of solar energetic particle injection timing from onset times near Earth. *Astrophys. J.* **626**, 1131. DOI. ADS.

Talebpour Sheshvan, N., Pohjolainen, S.: 2018, Visibility and origin of compact interplanetary radio type IV bursts. *Solar Phys.* **293**, 148. DOI. ADS.

Tan, L.C., Malandraki, O.E., Reames, D.V., Ng, C.K., Wang, L., Patsou, I., Papaioannou, A.: 2013, Comparison between path lengths traveled by solar electrons and ions in ground-level enhancement events. *Astrophys. J.* **768**, 68. DOI. ADS.

Torsti, J., Valtonen, E., Lumme, M., Peltonen, P., Eronen, T., Louhola, M., Riihonen, E., Schultz, G., Teittinen, M., Ahola, K., Holmlund, C., Kelhä, V., Leppälä, K., Ruuska, P., Strömmer, E.: 1995, Energetic particle experiment ERNE. *Solar Phys.* **162**, 505. DOI. ADS.

Vainio, R., Valtonen, E., Heber, B., Malandraki, O.E., Papaioannou, A., Klein, K.-L., Afanasiev, A., Agueda, N., Aurass, H., Battarbee, M., Braune, S., Dröge, W., Ganse, U., Hamadache, C., Heynderickx, D., Huttunen-Heikinmaa, K., Kiener, J., Kilian, P., Kopp, A., Kouloumvakos, A., Maisala, S., Mishev, A., Miteva, R., Nindos, A., Oittinen, T., Raukunen, O., Riihonen, E., Rodríguez-Gasén, R., Saloniemi, O., Sanahuja, B., Scherer, R., Spanier, F., Tatischeff, V., Tziotziou, K., Usoskin, I.G., Vilmer, N.: 2013, The first SEPServer event catalogue ∼ 68-MeV solar proton events observed at 1 AU in 1996 – 2010. *J. Space Weather Space Clim.* **3**(27), A12. DOI. ADS.

Van Hollebeke, M.A.I., Ma Sung, L.S., McDonald, F.B.: 1975, The variation of solar proton energy spectra and size distribution with heliolongitude. *Solar Phys.* **41**(1), 189. DOI. ADS.

Vršnak, B., Magdalenić, J., Zlobec, P.: 2004, Band-splitting of coronal and interplanetary type II bursts. III. Physical conditions in the upper corona and interplanetary space. *Astron. Astrophys.* **413**, 753. DOI. ADS.

Williams, M.J., Bureau, M., Cappellari, M.: 2010, The Tully–Fisher relations of early-type spiral and S0 galaxies. *Mon. Not. Roy. Astron. Soc.* **409**, 1330. DOI. ADS.

Williamson, J.H.: 1968, Least-squares fitting of a straight line. *Can. J. Phys.* **46**, 1845. DOI. ADS.

Xie, H., Ofman, L., Lawrence, G.: 2004, Cone model for halo CMEs: Application to space weather forecasting. *J. Geophys. Res. Space Phys.* **109**, A03109. DOI. ADS.

Xie, H., Mäkelä, P., Gopalswamy, N., St. Cyr, O.C.: 2016, Energy dependence of SEP electron and proton onset times. *J. Geophys. Res.* **121**, 6168. DOI. ADS.

York, D., Evensen, N.M., Martínez, M.L., De Basabe Delgado, J.: 2004, Unified equations for the slope, intercept, and standard errors of the best straight line. *Am. J. Phys.* **72**, 367. DOI. ADS.

Zhang, J., Dere, K.P.: 2006, A statistical study of main and residual accelerations of coronal mass ejections. *Astrophys. J.* **649**, 1100. DOI. ADS.

Zhang, J., Dere, K.P., Howard, R.A., Kundu, M.R., White, S.M.: 2001, On the temporal relationship between coronal mass ejections and flares. *Astrophys. J.* **559**, 452. DOI. ADS.